TECHNISCHE UNIVERSITÄT WIEN

VIENNA UNIVERSITY OF TECHNOLOGY

Diplomarbeit

# A microscopic approach to the imaginary $\alpha$-nucleus optical potential for magic nuclei.

ausgeführt am

Atominstitut der Österreichischen Universitäten

unter der Leitung von

Ao. Univ. Prof. Dipl-Ing. Dr. Helmut Leeb

durch

Michael Feher
Gartengasse 12/33
A-2351 Wr. Neudorf

Wien, August 2008 .....

# Abstract

The transition rates of nuclear reactions at low energy of several 100 keV are a key parameter for astrophysical models describing the evolution of stars. Particularly, for charged particle reactions reliable experimental data cannot be obtained at low energies due to the Coulomb barrier. Consequently one must take recourse to nuclear model calculations in order to predict the required quantities.

This diploma thesis focuses on the calculation of the imaginary part of the $\alpha$-nucleus optical potential within the nuclear structure approach for magic nuclei. In particular we consider $\alpha$-$^{16}$O scattering. A Fortran computer code was developed, based on the formulas given by F. Osterfeld, J.Wambach and V.A. Madsen [3], to calculate the imaginary part of the optical potential. For the target excitation states the RPA calculations from R. Kogler [12] and S. Krewald and J. Speth [20] where used.

The resulting imaginary part of the optical potential is given for $\alpha$-$^{16}$O scattering and is compared with the potentials obtained for $\alpha$-$^{40}$Ca in [3]. The comparison shows that the overall shape of the imaginary potential is reproduced quite well while the absolute values obtained for $^{16}$O are smaller than for $^{40}$Ca due to the considerably smaller number of open channels in the $\alpha$-$^{16}$O system.

We attempt to compare the associated cross sections with experimental data. It turns out that for the comparison with available reaction cross section data more involved RPA calculations would be required. For the comparison with differential elastic cross section data the real part of the potential should be calculated in addition.

Further work will aim at the extension of the calculation to non-magic nuclei and particles with spin. Optical potential formulae for spin 1/2 projection were given by H. Dermawan, F. Osterfeld and V.A. Madsen [17]. Extensions of the formulae to include QRPA-states are required for the treatment of non-magic target nuclei.

# Contents

**Motivation** **vii**

## I Theory 1

**1 The Model Space** **3**
1.1 The Shell Model . . . 3
1.2 Occupation Number Representation . . . 9
1.3 Hartree-Fock (HF) method . . . 14
1.4 Random Phase Approximation (RPA) . . . 17

**2 The Optical Potential** **21**
2.1 Elastic scattering . . . 21
2.2 The Optical Model . . . 25
2.3 General Optical Potential . . . 28
2.4 The $\alpha$-nucleus optical potential . . . 32

## II Implementation and Results 35

**3 Implementation** **37**
3.1 The Intermediate Potential . . . 37
3.2 The Green Function . . . 41
3.3 Transition form factor . . . 43
3.4 Results . . . 47

## III Program and Source Code 51

**4 The source code** **53**
4.1 General Description . . . 53
4.2 `config.f95` . . . 55
4.3 `rpaAmps.f95` . . . 55
4.4 `rho.f95` . . . 58

4.5 `alnucpot.f95` . . . . . 59
4.6 `formfact.f95` . . . . . 60
4.7 `intermedPot.f95` . . . . . 61
4.8 `green.f95` . . . . . 62
4.9 `optPot.f95` . . . . . 63

**IV Appendix** **65**

**A Derivations** **67**
A.1 Folding Potential . . . . . 67
A.2 The Green Function . . . . . 69
A.3 Spherical Multipole Expansion of the Nuclear Interaction . . . . . 71

**B Tables** **73**
B.1 $^{16}0$ RPA Amplitudes . . . . . 73

# List of Figures


1.1 Neutron and proton bound states . . . . . 5
1.2 Nuclear excitation level scheme . . . . . 8
1.3 Shell model excited state in Hartree-Fock and RPA . . . . . 17
1.4 Wood-Saxon and Harmonic Oscillator wave functions . . . . . 19

2.1 Energy dependence of diff. el. cross section . . . . . 25
2.2 Differential el. cross section . . . . . 28

3.1 M3Y nucleon-nucleon interaction . . . . . 38
3.2 $^4$He and $^{16}$O nucleon densities . . . . . 39
3.3 $\alpha$ - $^{16}$O interaction potential . . . . . 42
3.4 Intermediate optical Green function . . . . . 44
3.5 Effective $\alpha$-nucleon potential . . . . . 44
3.6 Multipole expansion of the $\alpha$-nucleon potential . . . . . 45
3.7 $3^-$RPA density functions . . . . . 46
3.8 $3^-$ state transition form factors . . . . . 46
3.9 Imaginary $\alpha$-$^{16}$O potential . . . . . 47
3.10 $\alpha$-$^{16}$O optical potential at 30 MeV . . . . . 48
3.11 Diff. el. cross section at 18MeV . . . . . 49

4.1 Module overview . . . . . 54
4.2 $\alpha$-nucleon interaction test . . . . . 60
4.3 Test of the Green Function . . . . . 63

# Motivation

In historic times numerous attempts where made to give an answer to the central questions of mankind, where do we come from and where will we go. In former time those questions were exclusively addressed from religions. All of them providing some kind of creation myth which tells us how everything began and how the end will be. With the development of science a different approach to these questions has become available.

Albeit the deep philosophical problems associated with those questions cannot be tackled by science, the scientific method based on basic laws of nature provides detailed knowledge of the evolution of the universe. At present we have a profound understanding of most observed phenomena like the creation and death of stars. Even though big progress [1] has been made in the study of the universe and the models used to explain the phenomena, there are still deficiencies and uncertainties in the models. Models in use describing the composition of the universe are strongly based on nuclear reaction data. They can be extracted from dedicated experiments and calculations which are then extrapolated to the relevant conditions under which the processes take place in the universe.

When we build models for the birth of stars and for the production of all elements starting from hydrogen important input for the models are the cross section data and transition rates for the relevant nuclear reactions. For the formation of the great variety of elements stars have to evolve through many burning phases. Elements up to iron can be generated in these burning phases via nuclear fusion and subsequent reactions, whereas heavier elements are generated via a series of neutron capture reactions and $\beta$-decays, which occur in different scenarios, e.g. the r-process in supernova explosions. An important process during helium burning is the $^{12}\mathrm{C}(\alpha,\gamma)^{16}\mathrm{O}$ reaction at energies of several 100keV. The measurement of such reactions at low energies is very difficult because of the small cross section due to the Coulomb barrier.

To obtain the required data for such low energies one usually takes recourse to measurements at higher experimentally accessible energies and extrapolate them to lower ones. Nuclear processes are highly non linear and such an extrapolation leads to significant uncertainties. Hence for a proper extrapolation the availability of reliable nuclear model calculations is important. In this diploma thesis we deal with a microscopic approach for the imaginary part of the $\alpha$-nucleus optical

potential. Especially, we consider the so-called nuclear structure approach. In this model a reasonable description of the target structure is crucial.

This diploma thesis is organized as follows. In chapter 1 we give a short introduction to the nuclear shell model and the methods of Random Phase Approximation (RPA) that will be used in the consecutive chapters to model the target nucleus. In chapter 2 we briefly review the essential concepts of scattering theory and the optical potential. Especially, we consider the calculation of the elastic scattering cross section. Based on the derivation of the optical potential by Feshbach [2] the basic formula of the nuclear structure approach [33] are given.

The aim of this diploma thesis is the implementation of an algorithm to calculate the (nonlocal) imaginary part of the optical potential. Similar work was done in the late 1970s and early 1980s by Osterfeld et. al. [3] who performed extended optical model calculations simulating the structure of the target nucleus by RPA wave functions. Considering the high computational effort for calculations with non-local potentials the results matched already quite well with the measurements. Since the mid 1980s no further calculations where performed along this line. Thus we redeveloped the methods and algorithms for the nuclear structure approach from Osterfeld et. al. and implemented the methods on modern hardware such that the results obtained by Osterfeld et. al. could be reproduced and further extended.

In chapter 3 we give a description of the methods and algorithms used in the software and the results that were achieved.

In chapter 4 we give a description of the source code, which will help to understand the different modules and their functions along with the methods and tests that where performed to evaluate their output. We also give a description of the options of the source code available through the configuration files as well as the syntax used in the input and output files.

# Part I

# Theory

# Chapter 1

# The Model Space

Since Rutherford first discovered 1911 the existence of the nucleus numerous experiments were conducted to study its properties and inner structure. Nuclear scattering experiments revealed very soon that the nucleus is composed of neutrons and protons which are bound together by the strong interaction. Even in the simplest picture the nucleus represents a quantum mechanical many-body problem. Hence ab-initio calculations starting from the nucleon-nucleon interaction are limited to the lightest nuclei. Therefore, for a theoretical description of the nucleus one has to take recourse to models, which provide a fair description of the most important features.

Several nuclear models have been developed emphasizing different properties of the nucleus. The liquid drop model focuses on the global features of nuclei. The nuclear shell model is a more sophisticated model, which explains the internal structure via an independent particle model. Going beyond the independent particle model collective excitations can e.g. be described via the Random Phase Approximation (RPA). Even though big advances have been made in nuclear physics, the inner structure and origin of the forces acting inside the nucleus are still not completely understood and give rise to a wide field of intense research.

## 1.1 The Shell Model

From nuclear scattering experiments we know that neutrons and protons in the nucleus are bound in discrete energy states. This indicates that the nucleus has a shell structure similar to the electron in the nuclear electric field.

The shell model assumes that the nucleons are moving independently in a mean field generated by the other nucleons. At a first glance the validity of independent particle motion is surprising because of the high nucleon density in the nucleus which implies strong forces between nucleons and should lead to correlations. However, such correlations are suppressed due to the Pauli principle which allows essentially only elastic scattering processes between nucleons in the

nucleus.

The nuclear mean field is an attractive single-nucleon potential which contains effectively all contributions from the other nucleons. Solving the corresponding single-nucleon Schrödinger equation yields the single-nucleon bound state energies and corresponding bound state wave functions. Choosing the proper number of energetically lowest bound states one can approximate the ground state of the nucleus in form of an antisymmetrized product of these single nucleon bound states. This assumption of the ground state in form of a so called Slater determinant is the basis of the Hartree-Fock method [4, 5]. It is the aim of the Hatree-Fock method to provide under this assumption the best mean field and wave functions for the nucleus. The optimization to find a self consistent solution is performed in several iterative steps.

Hartree-Fock calculations are numerically involved. Therefore, phenomenologically determined mean fields are frequently used. They are based on the following ideas. Their radial shape reflects the short range behavior of the strong force. In the interior of a nucleus the nucleons are tightly packed and the effective potential seen by a single nucleon will mainly stem from the neighboring nucleons. Thus the nuclear mean field will be almost constant within the nucleus and will quickly vanish beyond the surface. The nuclear potential is often approximated by a parametrized Wood-Saxon potential which fulfills these requirements,

$$V_{\mathrm{N}}(r) = \frac{V_0}{1 + e^{\frac{r-R_0}{a}}} \ , \tag{1.1}$$

where the mean radius of the nucleus is typically given by $R_0 = r_0 A^{1/3}$ with $A$ being the number of nucleons. It turned out, that the Wood-Saxon parameter $r_0 = 1.25$ fm and $a = 0.65$ fm yield very good results for almost all nuclei.

In addition to the attractive strong force the charged nucleons are also affected by the Coulomb force, which leads to a repulsive component $V_{\mathrm{C}}$ in the total potential. The repulsive Coulomb force weakens the potential and consequently there are less proton than neutron bound states in heavy nuclei. This agrees with the fact that in stable heavy nuclei the number of neutrons exceeds the number of protons where in light nuclei they are equal. In Fig.1.1 the effect of the Coulomb force on the mean field and the number of proton and neutron bound states is shown.

The Schrödinger equation for the motion of the nucleons within the mean field is

$$\left( -\frac{\hbar^2}{2\mu}\vec{\nabla}^2 + \int \mathrm{d}^3 r' \ V(\vec{r}, \vec{r'}) \right) \phi(\vec{r}) = E\phi(\vec{r}) \ , \tag{1.2}$$

where $\mu$ is the reduced mass of the nucleon within the nucleus. In general the nuclear mean field $V(r, r')$ is nonlocal due to the Pauli principle and the complexity of the nucleon-nucleon interaction. However, it is assumed that the nonlocal potential can be represented by an equivalent local potential that will result in

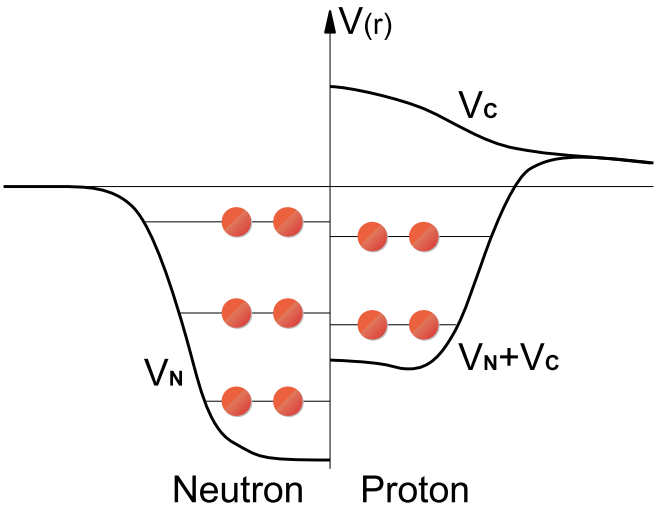


Figure 1.1: Neutron and proton bound states in a Wood-Saxon potential with Coulomb interaction.

the same bound state spectrum as the nonlocal one. Hence we can write

$$\left(-\frac{\hbar^2}{2\mu}\vec{\nabla}^2 + V(\vec{r})\right)\phi(\vec{r}) = E\phi(\vec{r}) \ . \tag{1.3}$$

The approximated equivalent local potential

$$V(\vec{r}) = V_{\mathrm{N}}(\vec{r}) + V_{\mathrm{C}}(\vec{r}) \tag{1.4}$$

is then given by its contributions from the Coulomb interaction $V_{\mathrm{C}}$ and the nuclear interaction $V_{\mathrm{N}}$.

Furthermore we assume spherical symmetry of the nucleus and its potentials which is a good approximation for magic nuclei. Non closed-shell nuclei, especially heavy ones, show significant deformations with either oblate or elongated shapes.

For the mathematical formulation the single-nucleon wave function $\phi(\vec{r})$ is expanded in spherical harmonics

$$\phi(\vec{r}) = \sum_{nl}\frac{1}{r}u_{nl}(r)\sum_{m=-l}^{m=l}Y_{lm}(\Omega) \ . \tag{1.5}$$

Inserting Eq. (1.5) into Eq. (1.3) one obtains for the radial part

$$\left(\frac{\hbar^2}{2\mu}\frac{\mathrm{d}^2}{\mathrm{d}r^2} - \frac{l(l+1)}{r^2} + \epsilon_{nl} - V(r)\right)u_{nl}(r) = 0 \ . \tag{1.6}$$

We search for bound states, which are solutions to Eq. (1.6) with negative energy $\epsilon_{nl}$ and fulfill also the boundary conditions $u_{nl}(r) \xrightarrow{r\to 0} 0$ and $u_{nl}(r) \xrightarrow{r\to\infty} 0$. The

solutions $u_{nl}(r)$ are orthogonal and can be normalized

$$\int_0^\infty \mathrm{d}r \; u_{nl}(r) \; u_{n'l}(r) = \delta_{n,n'} \; . \tag{1.7}$$

Hence they represent a system of orthonormal functions.

For fixed quantum numbers $n$ and $l$ the potential $V(r)$ can sustain no or several bound states each with a characteristic single-particle energy $\epsilon_{nl}$. The wave function associated with this set of quantum numbers $n$ and $l$ can be cast in the form

$$\phi_{nl}(\vec{r}) = \frac{1}{r} u_{nl}(r) \sum_{m_l=-l}^{m_l=l} \sum_{m_s=-1/2}^{m_s=1/2} a_{m_l,m_s} Y_{lm_l}(\Omega) \chi_{sm_s} \; , \tag{1.8}$$

where $Y_{lm_l}$ are the spherical harmonics and $\chi_{sm_s}$ are the spinor eigenfunctions. The amplitudes $a_{m_l,m_s}$ obey the relation

$$\sum_{m_l=-l}^{m_l=l} \sum_{m_s=-l/2}^{m_s=l/2} a_{m_l,m_s} a^*_{m_l,m_s} = 1 \; . \tag{1.9}$$

Considering all possible spin directions $m_s = \pm 1/2$ we can construct $4l+2$ linearly independent wave functions for each $\epsilon_{nl}$.

From experiments it is well established that some of the nucleon configurations are more stable than others. The most stable configurations are those, where either the number of neutrons or protons in the nucleus are magic numbers. Those magic numbers are 2, 8, 20, 28, 50, 82 and 126 for neutrons and 114 for protons. Nuclei where both the neutron and proton number are magic are even more stable and are called double magic nuclei. Such an increased stability occurs at the closure of a shell and is followed by an energy gap in the single nucleon spectrum.

If we compare the energy eigenvalues $\epsilon_{nl}$ for a simple local potential, e.g. the harmonic oscillator potential, and the number of nucleons that can occupy the corresponding states we are able to reproduce the first three magic numbers, while the simple picture fails to explain the higher ones. To predict the magic numbers above 20 a spin-orbit coupling is required. Thus the total interaction is given by

$$V(\vec{r}) = V_{\mathrm{N}}(\vec{r}) + V_{\mathrm{C}}(\vec{r}) + V_{\mathrm{SO}}(\vec{r}) \; , \tag{1.10}$$

where the spin-orbit term is

$$V_{\mathrm{SO}}(\vec{r}) = \left(\frac{\hbar}{\mu_\pi c}\right)^2 V_{\mathrm{SO}} \frac{1}{r} \frac{\mathrm{d}}{\mathrm{d}r} f(r) \vec{l}\vec{s} \, , \tag{1.11}$$

$$f(r) = \frac{1}{1 + e^{\frac{r-R_0}{a}}} \; . \tag{1.12}$$

Here $\vec{s}$ is the spin of the nucleon, $\vec{l}$ is the orbital angular momentum of the relative motion, $V_{\rm S}$ is the strength of the spin-orbit potential, and $\mu_\pi = 139.5$MeV is the pion mass.

Because of the spin-orbit term the orbital angular momentum $\vec{l}$ and the spin $\vec{s}$ are not conserved and consequently $m_l$ and $m_s$ are not anymore good quantum numbers. A proper set of eigenfunctions are generalized spherical harmonics which are given in terms of $Y_{lm_l}\chi_{sm_s}$,

$$\mathcal{Y}_{jlsm}(\Omega) = \sum_{m_l+m_s=m} \left[ \begin{array}{ccc} l & s & j \\ m_l & m_s & m \end{array} \right] Y_{lm_l}(\Omega)\chi_{sm_s} \tag{1.13}$$

where the squared bracket is the Clebsch-Gordan coefficient given by a standard 3j symbol. These state vectors $\mathcal{Y}_{jlsm}(\Omega)$ are eigenfunctions to the operators

$$\begin{aligned} \widehat{J}_z\mathcal{Y}_{jlsm}(\Omega) &= m\hbar\mathcal{Y}_{jlsm}(\Omega) \ , \\ \widehat{J}^2\mathcal{Y}_{jlsm}(\Omega) &= j(j+1)\hbar^2\mathcal{Y}_{jlsm}(\Omega) \ , \\ \widehat{L}^2\mathcal{Y}_{jlsm}(\Omega) &= l(l+1)\hbar^2\mathcal{Y}_{jlsm}(\Omega) \ , \\ \widehat{S}^2\mathcal{Y}_{jlsm}(\Omega) &= s(s+1)\hbar^2\mathcal{Y}_{jlsm}(\Omega) \ . \end{aligned} \tag{1.14}$$

The $\mathcal{Y}_{jlsm}(\Omega)$ are also eigenfunctions of the spin-orbit interaction $\widehat{L}\widehat{S}$ because of

$$\begin{aligned} \widehat{J}^2 &= \left(\widehat{L}+\widehat{S}\right)^2 \\ &= \widehat{L}^2 + 2\widehat{L}\widehat{S} + \widehat{S}^2 \ . \end{aligned} \tag{1.15}$$

Since $\mathcal{Y}_{jlsm}(\Omega)$ is eigenfunction to $\widehat{J}^2$, $\widehat{L}^2$ and $\widehat{S}^2$ it is also eigenfunction to $\widehat{L}\widehat{S}$,

$$\widehat{L}\widehat{S}\mathcal{Y}_{jlsm}(\Omega) = \frac{1}{2}\left[j(j+1) - l(l+1) - s(s+1)\right]\hbar\mathcal{Y}_{jlsm}(\Omega) \ . \tag{1.16}$$

The spin-orbit interaction splits the states for a particular $l$ into states with $j = l + 1/2$ which have a lower energy and $j = l - 1/2$ with a higher energy than the original level without spin-orbit coupling. The corresponding energy splitting from the spin-orbit coupling is displayed in Fig. 1.2. The variation of the energy levels by the spin-orbit interaction is clearly seen and gives rise to different energy gaps, thus explaining the magic numbers higher than 20.

Eq. (1.13) represents a transformation from the orthonormal set of $Y_{lm_l}(\Omega)\chi_{sm_s}$ states to the orthonormal set $\mathcal{Y}_{jlsm}(\Omega)$. All eigenfunctions belonging to the same energy eigenvalue have the same $n$, $l$ and $j$. Thus each eigenvalue of the Hamiltonian is $2j+1$ fold degenerated. The convention for the notation of the states is $n + 1(l)_j$, where the angular momentum is given by a letter s ($l = 0$), p ($l = 1$), d ($l = 2$), f ($l = 3$), g ($l = 4$), h ($l = 5$), .... Thus the spectroscopic notation of a single-nucleon state n=1, l=1, j=3/2 is given by $2p_{3/2}$.

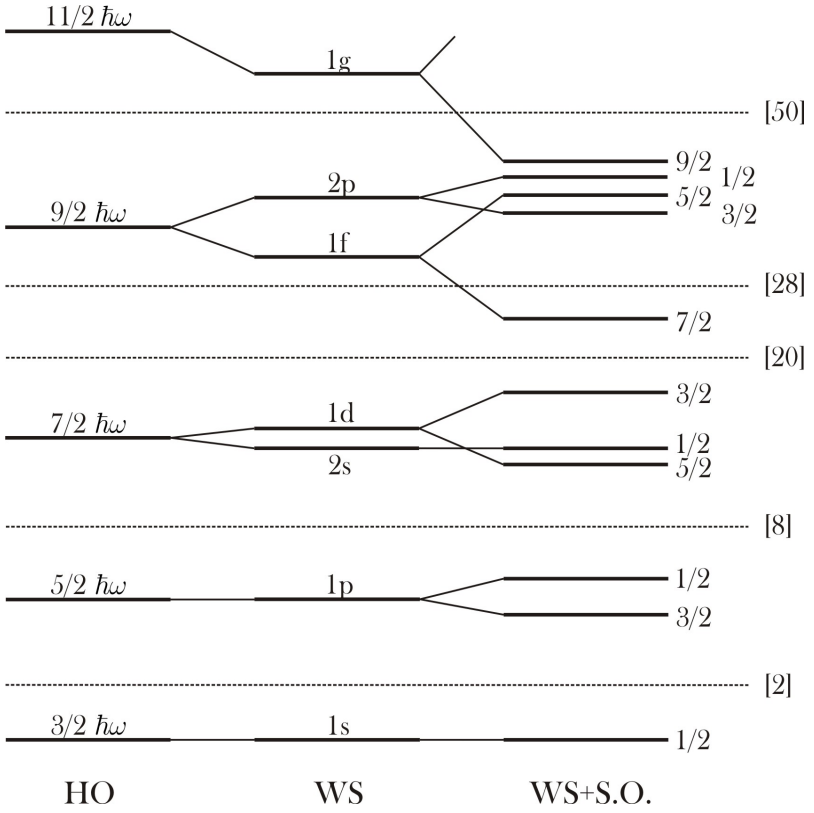


Figure 1.2: Level scheme derived from harmonic oscillator potential and Wood-Saxon potential with and without a spin-orbit term. The dashed lines show the energy gaps. The total number of states below this energy is given in squared brakes (Magic Numbers).

The ground state of a nucleus containing $N$ nucleons is in first order approximation the Slater determinant generated from the $N$ energetically lowest lying states. The energy of the highest occupied state defines the Fermi energy of the nucleus. Hence all states below the Fermi energy are occupied while those above are not. If we excite one nucleon from the ground state and leave all other nucleons in their single nucleon states we speak from a particle-hole excitation.

The nuclear mean field used to calculate the single nucleon states is itself generated by the other nucleons. Up to now the formalism employed does not include this self-consistent nature of the problem but considers the nuclear field as constant. This simple picture is certainly not true because the nucleons interact via the strong force and not all aspects of these two-body interactions can be accounted for by the mean field, which is a one-body operator. The non included parts of the two-body interaction gives rise to the residual interaction. Thus the realistic ground state is a mixture of Slater determinants of different single particle-hole configurations.

Such a configuration mixing has been successfully applied for the description of low-lying excited states of predominantly single-particle nature. For nuclear states of increased collectivity, i.e. many nucleons are involved in the excitation, this simple model is not suited.

In the next chapters we will discuss the random phase approximation (RPA) which assumes a more general basis composed of particles and holes. Including the residual interaction into the optimization process leads to a new ground and new excited states, latter partly of high collectivity. Especially for nearly closed-shell nuclei the RPA reproduces fairly well the low-energy spectra.

Before we give a short introduction to the RPA calculations we introduce in the next chapter the formalism of occupation numbers which will be used throughout the discussion of the RPA calculations.

## 1.2 Occupation Number Representation

We have seen in Sec. 1.1 that by solving the Schrödinger equation

$$\widehat{H}\phi_\lambda(\vec{r}) = \epsilon_\lambda \phi_\lambda(\vec{r}) \tag{1.17}$$

with the Hamiltonian

$$\widehat{H} = \left( -\frac{\hbar^2}{2\mu}\vec{\nabla}^2 + V(\vec{r}) \right) \tag{1.18}$$

we obtain a set of orthonormal single-particle wave functions $\phi_\lambda(\vec{r})$. Each of these wave functions $\phi_\lambda(\vec{r})$ is characterized by a complete set of quantum numbers $\lambda = \{ n, j, l, s, m_j \}$.

We assume that each fermion is in a specific single-particle state described by the single-particle wave function $\phi_\lambda(r)$ and characterized by the quantum

numbers $\lambda$. For a system of many fermions the total wave function must be antisymmetric with respect to the exchange of particles. A simple form of the many fermion wave function is the antisymmetrized product of single-particle states. For a two fermion system this wave function is given by

$$\Psi(\vec{r}_1, \vec{r}_2) = \frac{1}{2} \left[ \phi_{\lambda_1}(\vec{r}_1)\phi_{\lambda_2}(\vec{r}_2) - \phi_{\lambda_1}(\vec{r}_2)\phi_{\lambda_2}(\vec{r}_1) \right] \ , \tag{1.19}$$

where $\phi_{\lambda_1}$ and $\phi_{\lambda_2}$ are the single particle wave functions of the states associated with the quantum numbers $\lambda_1$ and $\lambda_2$. The spatial coordinates $\vec{r}_1$ and $\vec{r}_2$ are referring to the positions of the two particles, but may include also other degrees of freedom. For a set of $N$ particles the antisymmetrized wave function is the sum of $N!$ permutations of the particles which can conveniently be written in the form of the Slater determinant [6]

$$\Psi(\vec{r}_1, \vec{r}_2, \ldots, \vec{r}_N) = \frac{1}{\sqrt{N!}} \det \begin{vmatrix} \phi_{\lambda_1}(\vec{r}_1) & \phi_{\lambda_1}(\vec{r}_2) & \ldots & \phi_{\lambda_1}(\vec{r}_N) \\ \phi_{\lambda_2}(\vec{r}_1) & \phi_{\lambda_2}(\vec{r}_2) & \ldots & \phi_{\lambda_2}(\vec{r}_N) \\ \vdots & \vdots & \ddots & \vdots \\ \phi_{\lambda_N}(\vec{r}_1) & \phi_{\lambda_N}(\vec{r}_2) & \ldots & \phi_{\lambda_N}(\vec{r}_N) \end{vmatrix} \ . \tag{1.20}$$

The antisymmetrization of the wave function guarantees that two particles cannot occupy the same single-particle state. This can easily be deduced from the Slater determinant where the occurrence of two particles in the same state, $\lambda_i = \lambda_j$ leads to linearly dependent rows. Consequently the Slater determinant vanishes.

In the following we use the Dirac Bra-Ket notation[7] for a compact formulation. In the Bra-Ket notation the single particle wave functions $\phi_\lambda(\vec{r})$ is denoted by $\langle \vec{r} \,|\, \lambda \rangle$. Hence the single-particle state is characterized by $|\lambda\rangle$. Using this notation the state of an N-fermion system is given by

$$|\Psi_a\rangle = \mathscr{A} \prod_{i=1}^{N} \left| \lambda_i^{(a)} \right\rangle \ , \tag{1.21}$$

with the antisymmetrization operator $\mathscr{A}$ given by the Slater determinant of Eq. (1.20). The superscript $(a)$ denotes the decomposition of the state $|\Psi_a\rangle$ into single-particle states $|\lambda_i\rangle$ in . The same state $|\Psi_a\rangle$ can be written in the occupation number representation

$$|\Psi_a\rangle = \left| n_1^{(a)}, n_2^{(a)}, n_3^{(a)}, \ldots, n_i^{(a)}, \ldots, n_\infty^{(a)} \right\rangle \ , \tag{1.22}$$

where the occupation number $n_i$ is the number of particles in the single particle state $|\lambda_i\rangle$. For a fermionic system $n_i$ can either be 1 if the state is occupied or 0 if not.

The sum over all occupation numbers has to be equal to the total number of particles $N$,

$$\sum n_{\lambda_i}^{(a)} = N \ , \tag{1.23}$$

which is also know as the conservation of particle number. To make the representation unambiguous the entries of the occupation number notation need to be ordered. It is not important which system we choose to order the states but the order has to be fixed and may not be changed later. Let us assume we order the states according to their single particle energy $\epsilon_{\lambda_i}$ in ascending order. The single-particle state $|\lambda_3\rangle$ reads then in this representation

$$|\lambda_i\rangle \iff |0,0,1,0,0,...,0\rangle \ . \tag{1.24}$$

The two-particle state constructed from the single-particle states $|\lambda_2\rangle$ and $|\lambda_5\rangle$ can be written in occupation number presentation as

$$\begin{aligned} |\Psi\rangle &= \frac{1}{\sqrt{2}}\left[|\lambda_3\rangle_{(\vec{r}_1)}\,|\lambda_5\rangle_{(\vec{r}_2)} - |\lambda_3\rangle_{(\vec{r}_2)}\,|\lambda_5\rangle_{(\vec{r}_1)}\right] \\ &\iff |0,0,1,0,1,0,0,...,0\rangle \end{aligned} \tag{1.25}$$

Formally the occupation number representation spans a Fock space over the single-particle Hilbertspaces

$$\mathscr{F} = \mathrm{F}_0 \oplus \mathrm{F}_1 \oplus \mathrm{F}_2 \oplus \dots \ , \tag{1.26}$$

where $\mathrm{F}_N$ is the Hilbertspaces with $N$ single-particle states

$$\begin{aligned} \mathrm{F}_0 &= \{|0,0,0,0,\dots\rangle\} \\ \mathrm{F}_1 &= \{|1,0,0,0,\dots\rangle\,, |0,1,0,0,\dots\rangle\,, |0,0,1,0,\dots\rangle\,, \dots\} \\ \mathrm{F}_2 &= \{|1,1,0,0,\dots\rangle\,, |1,0,1,0,\dots\rangle\,, |0,1,1,0,\dots\rangle\,, \dots\} \ . \end{aligned} \tag{1.27}$$

We have introduced the vacuum state $|0,0,0,0,\dots\rangle$ with particle number $N=0$ which is denoted simply by $|0\rangle$. The states in occupation number representation obey the orthogonality relation

$$\langle n_1', n_2', n_3', \dots \mid n_1, n_2, n_3, \dots\rangle = \delta_{n_1',n_1}\ \delta_{n_2',n_2}\ \delta_{n_3',n_3}\ \dots \tag{1.28}$$

which also is valid for the vacuum state

$$\langle 0 \mid 0\rangle = 1 \tag{1.29}$$

We have seen that the states in occupation number representation are orthonormal. For the following it is essential to obtain a relationship between states with different particle numbers $N$. We therefore define the one-particle creation $c_i^\dagger$

and destruction operators $c_i$ that will raise or lower the occupation number for the state $i$.

$$\begin{aligned} c_i^\dagger \left|n_1, n_2, \ldots, n_i, \ldots\right\rangle &= (-1)^{s_i}\sqrt{n_i+1}\left|n_1, n_2, \ldots, n_i+1, \ldots\right\rangle \ , \\ c_i \left|n_1, n_2, \ldots, n_i, \ldots\right\rangle &= (-1)^{s_i}\sqrt{n_i}\left|n_1, n_2, \ldots, n_i-1, \ldots\right\rangle \ . \end{aligned} \tag{1.30}$$

The phase factor $s_i$ is given as the sum of the occupation numbers below the index $i$

$$s_i = \sum_{k=1}^{i-1} n_k \ . \tag{1.31}$$

For a fermionic system the admissible occupation numbers are 0 and 1. Therefore the application of the creation operator $c_i^\dagger$ on a particle state $n_i = 1$, or analogously of a destruction operator $c_i$ on an empty state $n_i = 0$ vanishes,

$$\begin{aligned} c_i^\dagger \left|n_1, n_2, \ldots, n_{i-1}, 1, n_{i+1}, \ldots\right\rangle &= 0 \ , \\ c_i \left|n_1, n_2, \ldots, n_{i-1}, 0, n_{i+1}, \ldots\right\rangle &= 0 \ . \end{aligned} \tag{1.32}$$

The application of the creation operator $c_i^\dagger$ on the vacuum state $|0\rangle$ generates the single-particle state $|\lambda_i\rangle$. With the creation operators we can construct the $N$-particle state by consecutive application of creation operators to the vacuum state

$$\left|\Psi_a\right\rangle = \prod_{i=1}^{N} c_{\lambda_i^{(a)}}^\dagger \left|0\right\rangle \ . \tag{1.33}$$

The $N$-particle state $|\Psi_a\rangle$ is the product of the $N$ ascending ordered single-particle creation operators $c_{\lambda_i^{(a)}}^\dagger$ applied to the vacuum state $|0\rangle$. For the ground state $|\Psi_0\rangle$ of the $N$-body system the creation operators of the $N$ energetically lowest states have to be applied to the vacuum state $|0\rangle$. Thus the occupation numbers of all single particle states below the Fermi energy are 1 while all other occupation numbers vanish.

$$\begin{aligned} \left|\Phi_0\right\rangle &= \prod_{\epsilon_\lambda \le \epsilon_F} c_\lambda^\dagger \left|0\right\rangle \\ &= \left|1_1, 1_2, 1_3, \ldots, 1_N, 0, 0, \ldots\right\rangle \end{aligned} \tag{1.34}$$

For fermions the creation and destruction operators obey the anticommutator relations $\{a, b\} = ab + ba$

$$\begin{aligned} \left\{c_i, c_j^\dagger\right\} &= \delta_{i,j} \ , \\ \left\{c_i, c_j\right\} &= \left\{c_i^\dagger, c_j^\dagger\right\} = 0 \ . \end{aligned} \tag{1.35}$$

The formalism allows the definition of the occupation number operator $c_i^\dagger c_i$ whose eigenvalue is the occupation number $n_i$

$$c_i^\dagger c_i \left|n_1, n_2, \ldots, n_i, \ldots\right\rangle = n_i \left|n_1, n_2, \ldots, n_i, \ldots\right\rangle \ . \tag{1.36}$$

This allows to define the particle number operator

$$\widehat{N} = \sum_i c_i^\dagger c_i \ . \tag{1.37}$$

In the following we mainly deal with single-particle and two-particle states and use the reduced notation $|s\rangle$ and $|st\rangle$, respectively,

$$\begin{aligned} |s\rangle &= |0,0,\ldots,0,n_s,0,\ldots\rangle = c_s^\dagger |0\rangle \ , \\ |st\rangle &= |0,0,\ldots,0,n_s,0,\ldots,0,n_t,0,\ldots\rangle = c_t^\dagger c_s^\dagger |0\rangle \ . \end{aligned} \tag{1.38}$$

With this definition we can write a one particle operator as

$$\mathscr{O} = \sum_{r,s} \langle r| \widehat{O} |s\rangle \, c_r^\dagger c_s \tag{1.39}$$

and a two-particle operator as

$$\mathscr{W} = \frac{1}{2} \sum_{rstu} \langle rs| \widehat{W} |tu\rangle \, c_r^\dagger c_s^\dagger c_u c_t \ . \tag{1.40}$$

We can now rewrite the Hamiltonian for the many body system

$$\begin{aligned} \mathscr{H} &= \mathscr{T} + \mathscr{V} + \mathscr{W} \\ &= \sum_i \frac{\hbar^2}{2\mu} \vec{\nabla}_i^2 + \sum_{r,s} \langle r| \widehat{V} |s\rangle \, c_r^\dagger c_s + \frac{1}{2} \sum_{rstu} \langle rs| \widehat{W} |tu\rangle \, c_r^\dagger c_s^\dagger c_u c_t \end{aligned} \tag{1.41}$$

in the occupation number notation. The many-body Hamiltonian Eq. (1.41) can be split into a one-particle interaction part that describes the movement of the particle in the mean field

$$\mathscr{H}_0 = \sum_{rs} \langle r| \left(\widehat{T} + \widehat{V}\right) |s\rangle \, c_r^\dagger c_s \tag{1.42}$$

and an effective two-body interaction representing the residual interaction between the particles.

$$\mathscr{H}_1 = \sum_{rstu} \langle rs| \widehat{W} |tu\rangle \, c_r^\dagger c_s^\dagger c_u c_t \ . \tag{1.43}$$

Thus the total Hamiltonian is

$$\mathscr{H} = \mathscr{H}_0 + \mathscr{H}_1 \ . \tag{1.44}$$

The ground state is eigenvalue of the Hamilton operator and satisfies the eigenvalue equation

$$\mathscr{H}_0 |\Psi_0\rangle = E_0 |\Psi_0\rangle$$

with the ground state energy $E_0$,

$$E_0 = \sum_{i=1}^{N} \epsilon_i \ . \tag{1.45}$$

Notice that the energy $E_0$ is not related to the total binding energy of the nucleus but it serves as a reference level for the excitation energies of the states $|\Psi_a\rangle$.

The nuclear shell model is based on a nuclear mean field which is obtained from the nucleon-nucleon interaction via some type of averaging procedure. An optimal choice of the nuclear mean field in $\mathscr{H}_0$ is obtained if the residual interaction acting on the ground state vanishes,

$$\mathscr{H}_1 \, |\Psi_0\rangle = 0 \ . \tag{1.46}$$

It is obvious that the relation will only be approximately satisfied for excited states $|\Psi_a\rangle$. If the number of nucleons in the nucleus is sufficiently high, the excitement of a single nucleon will have only a minor impact and we can assume that the change of the many-particle wave function and the r.h.s. of Eq. (1.46) is relatively small.

## 1.3 Hartree-Fock (HF) method

There exist several methods to determine the nuclear mean field from the nucleon-nucleon interaction. Among these the Hartree-Fock method is frequently used. The Hartree-Fock method starts from an initial single-particle potential and the associated wave functions of the single-particle states and allows to calculate the nuclear mean field from the nucleon-nucleon interaction in a self consistent procedure.

In this section we give a brief introduction to the HF method in second quantization and show the derivation of the nuclear mean field and the residual interaction from the two-particle interactions.

In the Hartree-Fock theory the ground state $|\Psi_0\rangle_{HF}$ is identified with the vacuum state $|0\rangle$. Thus we split the Fock space into two subspaces. One containing the states below the Fermi energy and one with the states above the Fermi energy

$$|\Psi_0\rangle = |1,1,...,1\rangle_{<\epsilon_F} \oplus |0,0,...\rangle_{>\epsilon_F} = |0\rangle_{HF} \ . \tag{1.47}$$

We define the particle and hole creation operators that act on the two subspaces,

$$a^\dagger_{\lambda_i} \ = \ c^\dagger_{\lambda_i} \qquad \epsilon_i > \epsilon_F \ , \tag{1.48}$$

$$b^\dagger_{-\lambda_i} \ = \ S_{\lambda_i} c_{\lambda_i} \quad \epsilon_i < \epsilon_F \ , \tag{1.49}$$

with the phase factor $S_i$,

$$S_i = (-1)^{j_i - m_i + t_i - m_{t_i}} \ . \tag{1.50}$$

The phase factor $S_i$ arises from the invariance against rotations of the particle-hole space and was given by J. Bell [8].

The hole creation operator $b^\dagger_{-\lambda_i}$ acting on the ground state $|\Psi_0\rangle$ generates a hole state in the Hartree-Fock ground state which is equivalent to the destruction of a particle below the Fermi energy. The hole creation operator creates an antiparticle state with third angular momentum and spin components inverted, i.e. with negative quantum number $-\lambda_i$. The antiparticle state absorbs the particle state and leaves behind a hole in the Hartree-Fock ground state. The negative value of the third components of the angular momentum and spin quantum numbers ensure that the laws of conservation remain valid for the particle-hole states.

When we apply the creation and destruction operators to the Hartree-Fock ground state we see, that the Hartree-Fock ground state contains neither holes nor particles

$$\begin{aligned} a^\dagger_{\lambda_i}|0\rangle_{HF} &= |\lambda_i\rangle_{HF} \ , \\ a_{\lambda_i}|0\rangle_{HF} &= 0 \ , \\ b^\dagger_{-\lambda_i}|0\rangle_{HF} &= |-\lambda_i\rangle_{HF} \ , \\ b_{-\lambda_i}|0\rangle_{HF} &= 0 \ . \end{aligned} \tag{1.51}$$

With the equivalent destruction operators we redefine the creation and destruction operators

$$c^\dagger_i = \theta(\epsilon_i-\epsilon_F)a^\dagger_i + \theta(\epsilon_F-\epsilon_i)S_{-i}b_{-i} \tag{1.52}$$

$$c_i = \theta(\epsilon_i-\epsilon_F)a_i + \theta(\epsilon_F-\epsilon_i)S_{-i}b^\dagger_{-i} \ , \tag{1.53}$$

where we replaced $\lambda_i$ by $i$.

To derive the nuclear mean field we rewrite the Hamilton Eq. (1.41) without external field in the second quantization

$$\mathscr{H} = \sum_{rs}\left\langle r\left|\widehat{T}\right|s\right\rangle c^\dagger_r c_s + \frac{1}{2}\sum_{rstu}\left\langle rs\left|\widehat{W}\right|tu\right\rangle c^\dagger_r c^\dagger_s c_u c_t \ . \tag{1.54}$$

With Wick's theorem [9] we can recast Eq. (1.54) in the form

$$\begin{aligned} \mathscr{H} &= \sum_{rs}\left\langle r\left|\widehat{T}\right|s\right\rangle\left[:c^\dagger_r c_s: + \underbrace{c^\dagger_r c_s}\right] \\ &+ \frac{1}{4}\sum_{rstu}\left\langle rs\left|\widehat{W}\right|tu\right\rangle\left[:c^\dagger_r c^\dagger_s c_t c_u: + :c^\dagger_r c_t:\underbrace{c^\dagger_s c_u}\right. \\ &- \left.:c^\dagger_r c_u:\underbrace{c^\dagger_s c_t} + \ldots + \underbrace{c^\dagger_r c^\dagger_s c_t c_u} - \underbrace{c^\dagger_r c^\dagger_s c_t c_u}\right] \ , \end{aligned} \tag{1.55}$$

where the colons denote the normal ordered product and the brackets below the creation and destruction operators represent a contraction. With the Hartree-Fock ground state all contractions $\underbrace{c^\dagger_r c_s}$ vanish except those where $r = s$ or $r$ and

$s$ denote states below the Fermi energy. So we can rewrite the Hamiltonian

$$\begin{aligned}
\mathscr{H} &= \widehat{H}_0 + \widehat{H}_1 + \widehat{H}_2 \ , \\
\widehat{H}_0 &= \sum_{r<F} \left\langle r \left| \widehat{T} \right| r \right\rangle + \frac{1}{2} \sum_{r,s<F} \left( \left\langle rs \left| \widehat{W} \right| rs \right\rangle - \left\langle rs \left| \widehat{W} \right| sr \right\rangle \right) \ , \\
\widehat{H}_1 &= \sum_{r \neq s} \left[ \left\langle r \left| \widehat{T} \right| s \right\rangle \sum_t \left( \left\langle rt \left| \widehat{W} \right| st \right\rangle - \left\langle rt \left| \widehat{W} \right| ts \right\rangle \right) \right] :c_r^\dagger c_s: \ , \\
\widehat{H}_2 &= \frac{1}{2} \sum_{rstu} \left\langle rs \left| \widehat{W} \right| tu \right\rangle :c_r^\dagger c_s^\dagger c_t c_u: \ .
\end{aligned} \tag{1.56}$$

Thus the Hamilton splits into a scalar $\widehat{H}_0$, a one-body interaction $\widehat{H}_1$ and a two-body interaction $\widehat{H}_2$. It is possible to find a set of states $|r\rangle$ that diagonalizes $\widehat{H}_0 + \widehat{H}_1$ and defines the energy eigenvalue equation of the Hartree-Fock theory

$$\left\langle r \left| \widehat{T} \right| s \right\rangle + \sum_t \left( \left\langle rt \left| \widehat{W} \right| st \right\rangle - \left\langle rt \left| \widehat{W} \right| ts \right\rangle \right) = \epsilon_r \delta_{rs} \ . \tag{1.57}$$

With the single-particle states which diagonalize $\widehat{H}_1$ we know the matrix elements of the kinetic energy and of the mean field in Eq. (1.42), i.e.

$$\begin{aligned}
\mathscr{H}_0 &= \widehat{T} + \widehat{V} \ , \\
\widehat{T} &= \sum_r \left\langle r \left| \widehat{T} \right| r \right\rangle c_r^\dagger c_r \ , \\
\widehat{V} &= \sum_r \sum_{s<F} \left( \left\langle rs \left| \widehat{W} \right| sr \right\rangle - \left\langle rs \left| \widehat{W} \right| rs \right\rangle \right) c_r^\dagger c_r \ .
\end{aligned} \tag{1.58}$$

Eq. (1.58) defines the nuclear mean field in the Hartree-Fock approximation. It is obtained by solving Eq. (1.57) usually starting from a first guess of the nuclear mean field. The associated single-particle bound state wave functions are then used to derive an improved nuclear mean field via Eq. (1.58), which can be used in Eq. (1.57) for the next iteration. On convergence of this iterative process a self-consistent mean field in Hartree-Fock approximation is obtained.

Within Hartree-Fock approximation the full many-particle Hamiltonian is given by

$$\mathscr{H} = E_0 + \sum_{r>F} \epsilon_r a_r^\dagger a_r - \sum_{s<F} \epsilon_s b_s^\dagger b_s + \frac{1}{2} \sum_{rstu} \left\langle rs \left| \widehat{W} \right| tu \right\rangle :c_r^\dagger c_s^\dagger c_t c_u: \ , \tag{1.59}$$

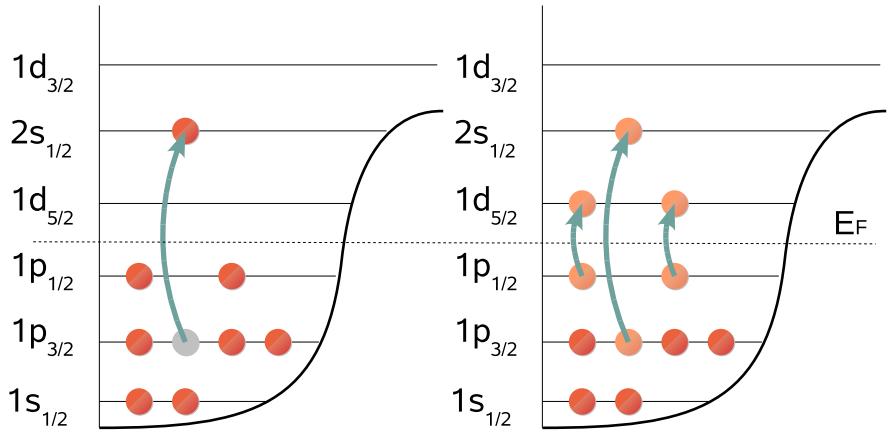


Figure 1.3: The left figure shows a single particle-hole excitation in the Hartree-Fock theory where on the right side we see a collective excitation in the RPA theory

where $E_0$ is the Hartree-Fock ground state energy,

$$\begin{aligned} E_0 &= \langle 0 | \mathscr{H} | 0 \rangle_{HF} \\ &= \sum_{r<F} \left\langle r \left| \widehat{T} \right| r \right\rangle + \frac{1}{2} \sum_{r,s<F} \left( \left\langle rs \left| \widehat{W} \right| rs \right\rangle - \left\langle rs \left| \widehat{W} \right| sr \right\rangle \right) . \end{aligned} \tag{1.60}$$

In the next section we will see how the Random Phase Approximation makes use of the concepts developed for the Hartree-Fock theory to calculate the nuclear excitation energies which include the contribution of the residual interaction $\widehat{H}_2$.

## 1.4 Random Phase Approximation (RPA)

We have outlined the Hartree-Fock method to estimate the nuclear mean field and ground state of the nucleus. The Hartree-Fock mean field is a good approximation for the low lying excitations of predominantly single-particle character. For the central scope of this diploma thesis, i.e. the calculation of microscopic optical potentials, a fairly good knowledge of the nuclear excitations of the target nucleus is needed. Hence a method is required which includes also the residual interaction $\mathscr{H}_2$. The RPA is such a method and in general provides improved excitation spectra compared to those obtained from the Hartree-Fock method.

The random phase approximation was first introduced by D. Bohm and D. Pines[10, 11] in 1953 to describe the collective behavior of electrons. The method is applicable to all kind of fermion systems. Especially it can be used to predict collective nuclear states. We will not give a detailed derivation of the RPA method but rather describe their concept and give the main results. A more detailed introduction into the RPA can be found in [9, 12].

In the framework of the RPA we start from a correlated ground state which is assumed to be the vacuum state of a quasi-particle operator $\widehat{Q}_n^\dagger$. The latter is a superposition of particle-hole creation and destruction operators, which will be defined below. As a consequence the occupation numbers of the single-particle states are no longer limited to the values 0 and 1. Further in the RPA the occupation numbers of the ground state $|\Psi_0\rangle$ are no longer 1 below the Fermi energy and 0 above. Hence the RPA ground state contains small particle-hole admixtures and the destruction operators applied to the RPA ground state no longer vanish,

$$\begin{aligned} a_i \,|\Phi_0\rangle &\neq 0 \,, \\ b_{-i} \,|\Phi_0\rangle &\neq 0 \,. \end{aligned} \tag{1.61}$$

Fig. 1.3 gives a schematic comparison of the generation of excited states in the Hartree-Fock theory and in the RPA. We see that in the Hartree-Fock theory each nucleon is represented by exactly one single-particle Hartree-Fock state. In the RPA theory the single-particle states may be occupied partly. The total number of nucleons is in both cases given by the sum of all occupation numbers and is conserved.

In this section we use for the RPA state vectors the Bra-Ket notation $|\Phi_n\rangle$ and for the single-particle states $|n\rangle$. The single particle state $|n\rangle$ can but do not need to be the Hartree-Fock states. It is assumed that the exact excitation state $|\Phi_n\rangle$ can be expanded in the basis of $|n\rangle$. In the RPA the harmonic oscillator (HO) wave functions are often used for the basis states $|n\rangle$. The HO functions are known to form a complete set which allows us to represent any function as an expansion of HO wave functions. The RPA ground state is required to contain only small particle-hole admixtures. Hence the ground state of the harmonic oscillator potential should approximate the RPA ground state quite well.

Fig. 1.4 shows the lowest lying neutron wave functions in $^{16}$O for a realistic Wood-Saxon potential and for the harmonic oscillator potential. We see that the radial wave functions of the corresponding $1s$ and $1p$ states differ only slightly so that the $^{16}$O ground state which contains 8 Neutrons in the $1s$ and $1p$ states can be approximated very well by the HO wave functions.

An exact calculation of the RPA states requires the inclusion of all basis vectors which is numerically not feasible. Therefore, in actual calculation only the first few states up to $3\hbar\omega$ are usually taken into account. This simplification represents the main limitation to the accuracy of the method. The quality of the calculations becomes better if the basis is extended.

For the RPA calculation we define the particle-hole creation and destruction operators as

$$\begin{aligned} \xi_{rs}^\dagger &= a_r^\dagger b_s^\dagger \\ \xi_{rs} &= a_r b_s \end{aligned} \tag{1.62}$$

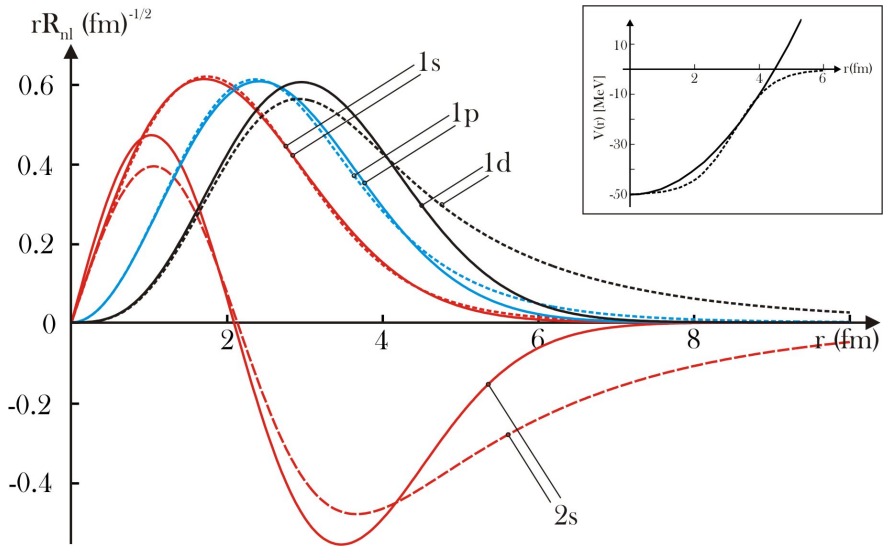


Figure 1.4: Comparison of $^{16}$O neutron wave functions derived from a realistic Wood-Saxon potential (solid line) and from an harmonic oscillator potential (dashed line)

where $\xi^\dagger_{rs}$ creates a particle-hole pair and $\xi_{rs}$ destroys one. The two operators conserve the total number of particles. As the RPA states consist of particle-hole admixtures the transition from the ground state $|0\rangle$ to the state $|n\rangle$ can no longer be described by a single particle-hole creation operator but has to be an admixture of the particle-hole creation and destruction operators

$$\widehat{Q}^\dagger_n = \sum_{rs} X^{(n)*}_{rs}\xi^\dagger_{rs} - Y^{(n)*}_{rs}\xi_{rs} \ . \tag{1.63}$$

The $X^{(n)*}_{rs}$ and $Y^{(n)*}_{rs}$ are the RPA amplitudes calculated within the RPA framework. In particular we can create the excited state $|\Psi_n\rangle$ from the ground state by application of the quasi particle creation operator

$$|\Psi_n\rangle = \widehat{Q}^\dagger_n |\Psi_0\rangle \ . \tag{1.64}$$

The application of any quasi particle destruction operator to the ground state vanishes

$$\widehat{Q}_n |\Psi_0\rangle = 0 \ . \tag{1.65}$$

To calculate the RPA amplitudes $X^{(n)*}_{rs}$ and $Y^{(n)*}_{rs}$ the commutator equations with the full Hamilton operator have to be evaluated

$$\left\langle n \left| \left[\mathscr{H}, \xi^\dagger_{rs}\right] \right| 0 \right\rangle = (E_n - E_0) X^{(n)}_{rs} \tag{1.66}$$

$$\left\langle n \left| \left[\mathscr{H}, \xi_{rs}\right] \right| 0 \right\rangle = (E_n - E_0) Y^{(n)}_{rs} \ , \tag{1.67}$$

where $E_n$ is the energy of the RPA state

$$\mathscr{H} |\Psi_n\rangle = E_n |\Psi_n\rangle \ . \tag{1.68}$$

Eq. (1.66) and Eq. (1.67) lead to the coupled system of equations for the RPA amplitudes

$$([E_0 + (\epsilon_r - \epsilon_s)] - E_n)X_{rs}^{(n)} = -\sum_{tu}\left(v_{rs;tu}\ X_{tu}^{(n)} + u_{rs;tu}\ Y_{tu}^{(n)}\right) \quad (1.69)$$

$$([E_0 - (\epsilon_r - \epsilon_s)] - E_n)Y_{rs}^{(n)} = \sum_{tu}\left(v_{rs;tu}^{*}\ X_{tu}^{(n)} + u_{rs;tu}^{*}\ Y_{tu}^{(n)}\right) , \quad (1.70)$$

with

$$v_{rs;tu} = S_{-s}S_{-u}\left(\left\langle t,-s\left|\widehat{W}\right|-u,r\right\rangle - \left\langle t,-s\left|\widehat{W}\right|r,-u\right\rangle\right) \quad (1.71)$$

$$u_{rs;tu} = S_{-s}S_{-u}\left(\left\langle -s,-u\left|\widehat{W}\right|r,t\right\rangle - \left\langle -s,-u\left|\widehat{W}\right|t,r\right\rangle\right) , \quad (1.72)$$

where $S$ is the phase given by Eq. (1.50) and the states $|-u,r\rangle$ are the two particle states where the negative quantum number represents a hole and the positive quantum number represents a particle state.

Eq. (1.69) and Eq. (1.70) form a system of equations of dimension $2N$ where $N$ is the number of basis functions taken into account. Theoretically this gives $2N$ possible solutions for the RPA vectors, where only half of the solutions belong to positive excitation energies $E_n$. The solutions with negative energies are considered unphysical and are discarded. The RPA states are normalized and form a system of orthonormal state vectors,

$$\langle \Psi_n \mid \Psi_m\rangle = \sum_{rs}\left[X_{rs}^{(n)}X_{rs}^{(m)*} - Y_{rs}^{(n)}Y_{rs}^{(m)*}\right] = \delta_{nm} . \quad (1.73)$$

The orthonormal RPA states allow us to microscopically evaluate nuclear states starting from the nucleon-nucleon interaction. The results obtained from the model are in fair agreement with the experimental spectra. The RPA model and it's states will be used in the following section to derive the imaginary part of the $\alpha$-$^{16}$O optical potential.

# Chapter 2

# The Optical Potential

## 2.1 Elastic scattering

In the following we consider the elastic scattering of a projectile with mass $m_1$ and incoming energy $E_{\mathrm{Lab}}$ of a target nucleus of mass $m_2$ at rest. In the elastic scattering process the collision of particles occur without change of the internal structure of the collision partners, which is equivalent with the fact that there is no exchange of energy between the colliding particles in the c.m. system. Due to exchange of momentum a scattering angle between the incident and the scattered projectile will be observed. The scattering problem is usually treated in the center of mass frame which requires the separation of the center of mass motion from the Hamiltonian. This leads to the Schrödinger equation of the relative motion in the center of mass frame

$$\left(-\frac{\hbar^2}{2\mu}\vec{\nabla}^2 + V(r)\right)\psi(\vec{r}) = E\psi(\vec{r}) \ , \tag{2.1}$$

with the reduced mass $\mu = m_1 m_2/(m_1 + m_2)$, the nuclear interaction potential $V(r)$ and the energy of the relative motion in the c.m. frame

$$E = E_{\mathrm{Lab}}\frac{m_2}{m_1 + m_2} \ . \tag{2.2}$$

For elastic scattering the length of the wave vector $\vec{k}$ of the incoming and outgoing particle wave is conserved and is given by

$$k = \sqrt{\frac{2\mu E}{\hbar^2}} \ . \tag{2.3}$$

At positive energies $E$ and with a spherical symmetric potential $V(r)$ the scattering solutions at asymptotic distances can be expressed as superposition of plane and spherical waves

$$\psi(r,\theta) \xrightarrow{r\to\infty} e^{ikr\cos\theta} + f(\theta)\frac{e^{ikr}}{r} \ . \tag{2.4}$$

Here the first term describes an incoming plan wave in $z$ directions and the second term describes an outgoing spherical wave with the complex scattering amplitude $f(\theta)$, where $\theta$ is the angle between the incoming and outgoing wave.

In quantum mechanics the square of the wave functions $|\psi(r)|^2$ is identified with the probability density. In general the integral of the probability density is normalized to 1 which is not possible for the wave functions of Eq. (2.4). Scattering states are usually normalized to the delta function

$$\int \mathrm{d}^3 r \ \psi(\vec{k},\vec{r})\psi^*(\vec{k}',\vec{r}) = \delta(\vec{k}-\vec{k}') \ . \tag{2.5}$$

An alternative treatment of the scattering can be performed by the use of wave packets, which provide a more realistic description of the actual process. In this formulation the wave functions are square integrable and can be normalized to 1. However it requires the solution of the time dependent Schrödinger equation, which leads to additional difficulties. We therefore use the formulation with stationary states and refer for the wave packet formulation to standard text books in quantum mechanics (e.g.[13, 14]).

The probability current of the wave function $\psi(\vec{r})$ is

$$\vec{j} = -\frac{i\hbar}{2\mu}\left(\psi^*\vec{\nabla}\psi - \psi\vec{\nabla}\psi^*\right) \ . \tag{2.6}$$

With Eq. (2.4) we find for the incoming and outgoing waves the probability current at asymptotic distances

$$j_{\mathrm{in}} = \frac{\hbar k}{\mu} \ , \tag{2.7}$$

$$j_{\mathrm{out}}(\theta) = \frac{\hbar k}{\mu}\frac{|f(\theta)|^2}{r^2} \ . \tag{2.8}$$

From the incoming and outgoing probability current we can calculate the differential elastic cross section

$$\frac{\mathrm{d}\sigma}{\mathrm{d}\Omega} = \frac{r^2 j_{\mathrm{out}}}{j_{\mathrm{in}}} = |f(\theta)|^2 \ . \tag{2.9}$$

The complex scattering amplitude $f(\theta)$ plays a central role in all cross section calculations. It connects the experimental differential cross section data to the nuclear model calculations.

To derive an expression for the complex scattering amplitude $f(\theta)$ from the nuclear interaction potential, we start by expanding $\psi(r)$ in terms of radial wave functions $u_l(r)$ and the Legendre polynomials $P_l(\cos\theta)$

$$\psi(\vec{r}) = \frac{1}{kr}\sum_{l=0}^{\infty}(2l+1)i^l u_l(r)P_l(\cos\theta) \ . \tag{2.10}$$

Inserting Eq. (2.10) into the Schrödinger equation (2.1) yields the differential equation for the radial wave functions $u_l(r)$.

$$\left(\frac{\mathrm{d}^2}{\mathrm{d}r^2} - \frac{l(l+1)}{r^2} - \frac{2\mu}{\hbar^2}V(r) + k^2\right) u_l(r) = 0 \ . \tag{2.11}$$

We consider the nuclear interaction potential $V(r)$ to be short ranged so that the potential vanishes faster than $1/r$ in the asymptotic limit. At asymptotic distances the radial wave function $u_l(r)$ is then composed of spherical incoming and outgoing waves

$$\begin{aligned} u_l(r) &\xrightarrow{r\to\infty} u_l \sin(kr - \frac{\pi}{2}l + \delta_l) \\ &= u_l \frac{i^{-l}e^{i\delta_l}e^{ikr} - i^l e^{-i\delta_l}e^{-ikr}}{2i} \ , \end{aligned} \tag{2.12}$$

where the phase factor $\pi l/2$ stems from the asymptotic forms of the spherical Bessel- and Neumann-functions. The asymptotic form of Eq. (2.10) is then

$$\psi(r) \xrightarrow{r\to\infty} \frac{1}{2ikr}\sum_{l=0}^{\infty}(2l+1)\left(u_l e^{i\delta_l}e^{ikr} - (-1)^l u_l e^{-i\delta_l}e^{-ikr}\right) P_l(\cos\theta) \ . \tag{2.13}$$

To expand Eq. (2.4) in Legendre polynomials we use the relation

$$e^{ikr\cos\theta} = \sum_{l=0}^{\infty}(2l+1)i^l j_l(kr)P_l(\cos\theta) \tag{2.14}$$

with the spherical Bessel functions $j_l(kr)$ and their asymptotic limit

$$\begin{aligned} j_l(kr) &\xrightarrow{r\to\infty} \frac{\sin(kr - \frac{\pi}{2}l)}{kr} \\ &= i^{-l}\frac{e^{ikr} - (-1)^l e^{-ikr}}{2ikr} \ . \end{aligned} \tag{2.15}$$

For the scattering amplitude $f(\theta)$ we use the expansion

$$f(\theta) = \sum_{l=0}^{\infty}(2l+1)f_l P_l(\cos\theta) \ . \tag{2.16}$$

Thus we can rewrite Eq. (2.4) in partial wave expansion

$$\psi(\vec{r}) \xrightarrow{r\to\infty} \frac{1}{2ikr}\sum_{l=0}^{\infty}(2l+1)\left((-1)^{l+1}e^{ikr} + (1+2ikf_l)e^{-ikr}\right) P_l(\cos\theta) \ . \tag{2.17}$$

The coefficients for $\exp(ikr)$ and $\exp(-ikr)$ can be extracted by comparing Eq. (2.13) and Eq. (2.17)

$$\begin{aligned} (-1)^{l+1} &= u_l e^{i\delta_l} \ , \\ (1+2ikf_l) &= -(-1)^l u_l e^{-i\delta_l} \ . \end{aligned} \tag{2.18}$$

Solving this for the two variables $u_l$ and $f_l$ yields

$$\begin{aligned} u_l &= (-1)^{l+1} e^{-i\delta_l} \\ f_l &= \frac{1}{2ik}\left(e^{i2\delta_l}-1\right) \ . \end{aligned} \tag{2.19}$$

The total complex scattering amplitude $f(\theta)$ is then given as the sum of contributions for all angular momenta $l$

$$f(\theta) = \frac{1}{2ik}\sum_{l=0}^{\infty}(2l+1)\left(e^{i2\delta_l}-1\right)P_l(\cos\theta) \ . \tag{2.20}$$

With Eq. (2.20) the differential elastic cross section is obtained

$$\begin{aligned} \frac{\mathrm{d}\sigma}{\mathrm{d}\theta} &= |f(\Omega)|^2 \qquad (2.21) \\ &= \frac{1}{4k^2}\sum_{l,l'=0}^{\infty}(2l+1)(2l'+1)\left(e^{i2\delta_l}-1\right)\left(e^{i2\delta_{l'}}-1\right)P_l(\cos\theta)P_{l'}(\cos\theta) \ . \end{aligned}$$

The angular integral of the differential elastic cross section $\mathrm{d}\sigma/\mathrm{d}\Omega$ leads to the total elastic cross section $\sigma_{\mathrm{el}}$

$$\begin{aligned} \sigma_{\mathrm{el}} &= 2\pi\int_{-1}^{1}\mathrm{d}(\cos\theta)\frac{\mathrm{d}\sigma}{\mathrm{d}\Omega} = \frac{\pi}{k^2}\sum_{l=0}^{\infty}(2l+1)\left|e^{i2\delta_l}-1\right|^2 \\ &= \frac{4\pi}{k^2}\sum_{l=0}^{\infty}(2l+1)\sin^2\delta_l \ . \end{aligned} \tag{2.22}$$

Eq. (2.21) relates the differential elastic cross section to the phase shift $\delta_l$ obtained from nuclear model calculations. To derive the phase shift $\delta_l$ from the nuclear interaction potential $V(r)$ one has to solve the radial Schröedinger equation (2.11) for a given $l$. The phase shift is then obtained from the asymptotic behavior of the regular solution.

So far we only treated elastic scattering. Similar to classical scattering the energy of the relative motion is not conserved if the structure of the colliding partners changes in the scattering process. In Sec. 1.1 we saw that the nucleus can be in different states each associated with a certain excitation energy. The transition from one state into another one is thus associated with a characteristic change of the relative motion energy. In the next chapter we show how a complex potential $V(r)$ can be used to account for the loss of probability current in the elastic channel due to inelastic processes.

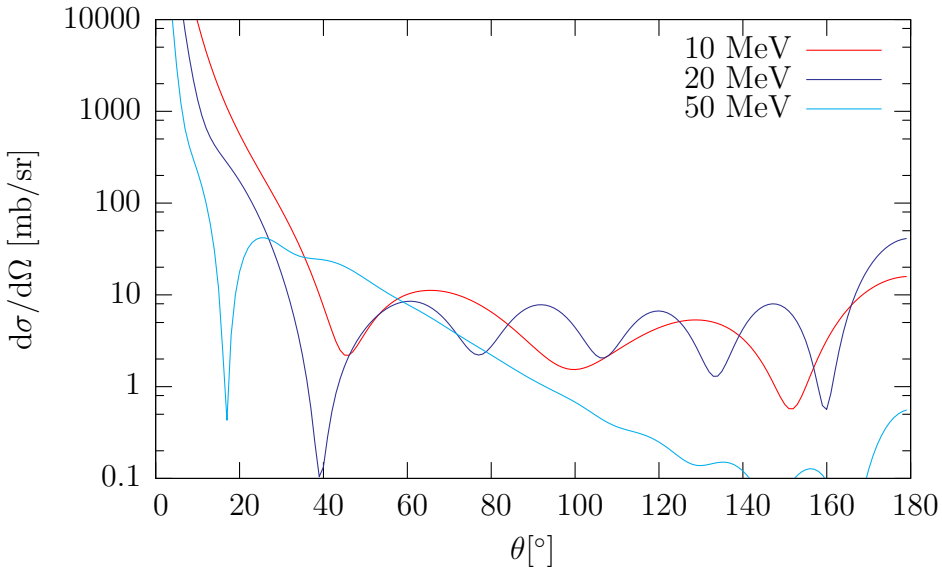


Figure 2.1: Energy dependence of the differential elastic cross section for $\alpha$-$^{16}$O scattering with a realistic Wood-Saxon interaction potential

## 2.2 The Optical Model

The nuclear interaction $V(r)$ is a key input to all nuclear reaction calculations. In principle it is a many-body operator for which exact solutions of the full many-body problem are required, which in full rigorousity are not feasible today. A very efficient approach to describe simple elastic scattering is provided by the so-called Optical Potential which is an effective one-body operator describing the main features of the collision process. The derivation of the interaction potential from the basic NN interaction is rather complicated and is equivalent to the solution of the many-body problem. A more pragmatic way is the use of a phenomenological optical potential which describes the elastic scattering cross section fairly well. The optical potential provides an energy averaged description, hence resonant behaviors are not reproduced. This is also true for non-elastic reactions which are included globally in the model.

The scattering observables reproduced by the optical potential are total and differential elastic cross section. In Sec. 2.1 we outlined how the elastic cross section can be extracted from the solution of the Schrödinger equation for a given potential $V(r)$. It is obvious from Eq. (2.1) that the solutions of the Schrödinger equation and consequently also the elastic cross section vary with energy. In Fig. 2.1 the typical energy and scattering angle dependence of the differential elastic cross section is show.

Beside the elastic scattering, inelastic scattering occurs when at least one of the reaction partners gets excited or the composition is changed in the scattering

process. The energy

$$\Delta\epsilon_{i,f} = \epsilon_f - \epsilon_i \tag{2.23}$$

which is necessary to excite the nucleus from its initial state to the final state has to be compensated by the relative motion energy. Hence, the initial relative motion wave vector $\vec{k}_i$ is changed into $\vec{k}_f$ with a different length.

The formation of an exited compound nucleus is only possible when the incident energy of the target is above the excitation energy $\Delta\epsilon_{i,f}$. All energetically allowed transitions are denoted as open channels and the energetically forbidden transitions as closed channels. The elastic scattering process proceeds in the elastic channel and all other processes represent transitions to a non-elastic channel. With rising incident energy $E$ the number of open channels increases and the contribution of non-elastic scattering to the overall scattering process becomes more important.

The transition rates to other reaction channels is given by the non-elastic cross section $\sigma_{\text{non}}$. If one of the collision partners is electrically neutral, an angle integrated elastic cross section exists

$$\sigma_{\text{el}}^{f} = \int \mathrm{d}\Omega \frac{\mathrm{d}\sigma}{\mathrm{d}\Omega} \ . \tag{2.24}$$

Here f denotes the form-elastic cross section which is obtained from the optical potential. Thus one can define the total reaction cross section

$$\sigma_{\text{tot}} = \sigma_{\text{el}}^{f} + \sigma_{\text{non}} \tag{2.25}$$

which represents a measure for reactions of the target nucleus in the beam. Especially at low neutron energies, measurements of the elastic cross section $\sigma_{\text{el}}$ differ from the form-elastic cross section $\sigma_{\text{el}}^{f}$ due to the occurrence of compound elastic scattering $\sigma_{\text{el}}^{c}$

$$\sigma_{\text{el}} = \sigma_{\text{el}}^{f} + \sigma_{\text{el}}^{c} \ . \tag{2.26}$$

Compound elastic scattering is essentially a non-elastic process which proceeds via the formation of an excited compound nucleus and its subsequent decay into the elastic channel. Thus it is useful to split the non-elastic cross section

$$\sigma_{\text{non}} = \sigma_{\text{el}}^{c} + \sigma_{\text{r}} \ , \tag{2.27}$$

where $\sigma_{\text{r}}$ is the reaction-cross section for transitions into all non-elastic reaction channels. The total cross section can then be given in terms of actually measured observables

$$\sigma_{\text{tot}} = \sigma_{\text{el}} + \sigma_{\text{r}} \ . \tag{2.28}$$

In case of charged particle collision the compound-elastic contribution is much smaller and usually neglected. However, it must be remarked that for charged particle scattering neither the angle integrated elastic nor the total-cross section exist in terms of simple integration.

The phenomenological optical model determines the elastic scattering amplitudes and elastic cross sections for a given interaction potential $V(r)$. The model does not explicitly take into account the non-elastic channels but allows to calculate the total non-elastic cross section which accounts for all non-elastic reactions. The non-elastic cross section thus describes the loss of probability flux in the elastic channel due to non-elastic processes.

To account for this loss of probability flux the optical potential must be complex-valued

$$V(r) = U(r) + iW(r) \ . \tag{2.29}$$

The effect of a complex potential is seen when we write down the continuity equation for the probability current

$$\begin{aligned} \vec{\nabla}\vec{j}(\vec{r}) &= \frac{\hbar}{i2\mu}\left(\psi^*(\vec{r})\vec{\nabla}^2\psi(\vec{r}) - \psi(\vec{r})\vec{\nabla}^2\psi^*(\vec{r})\right) \\ &= \frac{1}{\hbar}\left(\psi^*(\vec{r})W(\vec{r})\psi(\vec{r}) + \psi(\vec{r})W(\vec{r})\psi^*(r)\right) \\ &= \frac{2}{\hbar}\left|\psi(\vec{r})\right|^2 W(\vec{r}) \ , \end{aligned} \tag{2.30}$$

where we have used the two relations from the Schrödinger equation

$$\begin{aligned} \frac{\hbar^2}{2\mu}\vec{\nabla}^2\psi(\vec{r}) &= \left[U(\vec{r}) - E + iW(\vec{r})\right]\psi(\vec{r}) \ , \\ \frac{\hbar^2}{2\mu}\vec{\nabla}^2\psi^*(\vec{r}) &= \left[U(\vec{r}) - E - iW(\vec{r})\right]\psi^*(\vec{r}) \ . \end{aligned} \tag{2.31}$$

Integrating the continuity equation (2.30) and making use of the Gauss theorem yields

$$\oint_A \mathrm{d}^2\vec{r}\ \vec{j}(\vec{r}) = \frac{2}{\hbar}\int_V \mathrm{d}^3\vec{r}\ \rho(\vec{r})W(\vec{r}) \ . \tag{2.32}$$

The left hand side of Eq. (2.32) gives the net probability current through the closed surface $A$ which we identify with the reaction cross section

$$\sigma_\mathrm{r} \propto -\frac{2}{\hbar}\int_V \mathrm{d}^3\vec{r}\ \rho(\vec{r})W(\vec{r}) \tag{2.33}$$

From Eq. (2.32) we see that the reaction cross section is proportional to the negative convolution of the complex potential $W(\vec{r})$ with the density function $\rho(\vec{r}) = |\psi^2(\vec{r})|$. As the reaction cross section is always positive the integral on the right hand side of Eq. (2.32) has to be negative or 0. The probability density function $\rho(\vec{r})$ is a positive valued function thus the imaginary part of the optical potential $W(\vec{r})$ has to be predominantly negative. The imaginary part may contain positive areas as long as the integral remains negative.

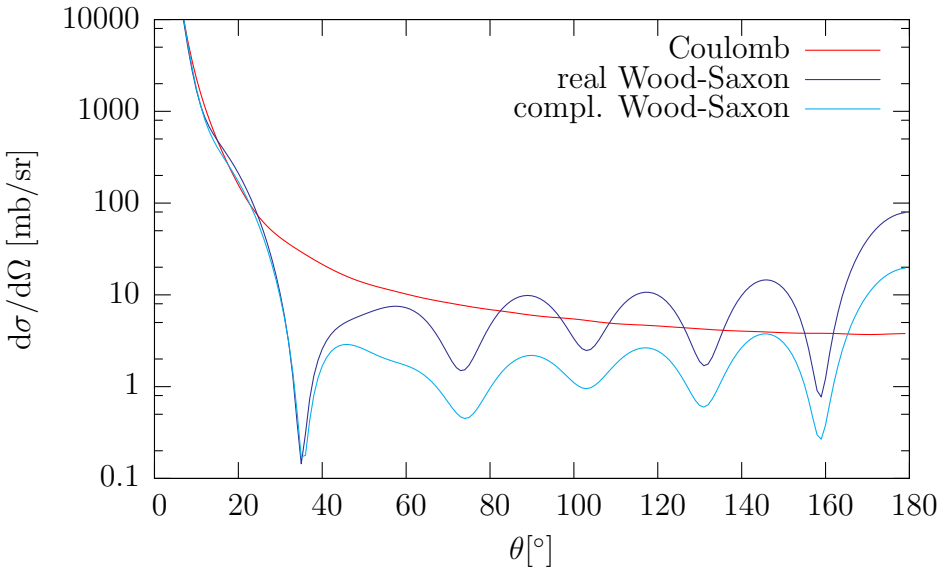


Figure 2.2: Differential elastic cross section derived from a pure Coulomb potential, a real Wood-Saxon and a complex Wood-Saxon potential at 18MeV incident energy. The Wood-Saxon potential parameters are $R_0 = 3.14$fm and $a = 0.65$fm.

Fig. 2.2 compares the differential elastic cross section $\mathrm{d}\sigma/\mathrm{d}\Omega$ for a real Coulomb potential and two Wood-Saxon type potentials combined with the Coulomb potential.

$$V(r) = V_{\mathrm{C}}(r) + \frac{-52.88 - [i3.00]}{1 + e^{\frac{r-R_0}{a}}} \tag{2.34}$$

The differential elastic cross section of the Wood-Saxon type potential is shown with and without the complex component. It shows the typical oscillations known from differential elastic cross section measurements. For low incident energies the complex part of the optical potential is small compared to the real part as only a few open channels exist. A complex component in the order of 10% of the real part reduces the elastic cross section without significantly changing the oscillations.

## 2.3 General Optical Potential

The general optical potential was first derived by Feshbach [2] in 1958 and has been further developed by several authors [3, 15–18] in the past. We briefly recall the original derivation of the so called general optical potential which allows us to connect the optical model to the nuclear shell model from chapter 1.

In nonelastic scattering either the projectile $\mathbf{A}$ or the target $\mathbf{B}$ or both change their states during the scattering process. To describe the process $\mathbf{A} + \mathbf{B} \rightarrow \mathbf{A}' + \mathbf{B}'$ we must include the target and projectile wave function into the calculations

explicitly. For a compact formulation we again use Dirac Bra-Ket[7] notation in the following

$$|\Psi_i\rangle = \left|\psi_i^{AB}\right\rangle |k_i\rangle \ . \tag{2.35}$$

The channel state $|\Psi_i\rangle$ is given as the product state of the projectile-target state $\left|\psi_i^{AB}\right\rangle$ and the relative motion state $|k_i\rangle$. The projectile-target state $\left|\psi_i^{AB}\right\rangle$ includes all internal degrees of freedom, i.e. all internal coordinates, total angular momentum, spin and isospin.

The total scattering state $|\Psi\rangle$ is a superposition of all possible channel states

$$|\Psi\rangle = \sum_i |\Psi_i\rangle = \sum_i \left|\psi_i^{AB}\right\rangle |k_i\rangle \ . \tag{2.36}$$

The sum $i$ runs here over all open channels where $i = 0$ denotes the elastic channel. The total scattering state $|\Psi\rangle$ satisfies the Schrödinger equation of the whole scattering system,

$$\widehat{H}\,|\Psi\rangle = E\,|\Psi\rangle \tag{2.37}$$

$$\widehat{H} = \widehat{H}^{AB} + \widehat{T}_0 + \widehat{V} \ , \tag{2.38}$$

where the total Hamilton operator $\widehat{H}$ splits into the projectile-target Hamiltonian $\widehat{H}^{AB}$, the kinetic energy operator $\widehat{T}_0$ and the interaction $\widehat{V}$ between the projectile and the target. The projectile-target states $\left|\psi_i^{AB}\right\rangle$ are eigenstates of the projectile-target Hamiltonian

$$\widehat{H}^{AB} \ \left|\psi_i^{AB}\right\rangle = \epsilon_i^{AB} \left|\psi_i^{AB}\right\rangle \tag{2.39}$$

and the relative motion vector $|k_i\rangle$ is an eigenstate of the kinetic energy operator

$$\widehat{T}_0\,|k_i\rangle = \frac{\hbar^2 k_i^2}{2\mu_i}\,|k_i\rangle \ . \tag{2.40}$$

The projectile-target interaction $\widehat{V}$ couples the channel states $|\Psi_i\rangle$

$$\left(E - \epsilon_i^{AB} - \frac{\hbar^2 k_i^2}{2\mu_i}\right)|\Psi_i\rangle = \sum_j V_{ji}\,|\Psi_j\rangle \tag{2.41}$$

with

$$V_{ji} = \langle\Psi_j|\,\widehat{V}\,|\Psi_i\rangle \ . \tag{2.42}$$

The projectile-target state $\left|\psi_i^{AB}\right\rangle$ incorporates all degrees of freedom of the nuclear reaction except the relative motion. We know that this state belongs to the composition $AB$ where the projectile is in the state $\left|\psi_i^{A}\right\rangle$ and the target is in the state $\left|\psi_i^{B}\right\rangle$.

Neglecting the antisymmetrization between projectile and target nucleons, the projectile-target state $\left|\psi_i^{AB}\right\rangle$ can be written in product form

$$\left|\psi_i^{AB}\right\rangle = \left|\psi_n^A\right\rangle \left|\psi_m^B\right\rangle \ . \tag{2.43}$$

The state vector of each collision partner fulfills the respective Schrödinger equation

$$\widehat{H}^A \left|\psi_n^A\right\rangle = \epsilon_n^A \left|\psi_n^A\right\rangle \ , \tag{2.44}$$
$$\widehat{H}^B \left|\psi_m^B\right\rangle = \epsilon_m^B \left|\psi_m^B\right\rangle \ , \tag{2.45}$$

where each collision partner has it's own set of eigenstates denoted by the subscripts $m$ and $n$. The product state $\left|\psi_i^{AB}\right\rangle$ is constructed from the possible eigenstate combinations where the index $i$ runs over all possible combinations $n, m$.

In this diploma thesis we consider only excited target states of the target nucleus without stripping or pickup processes. The numbers of nucleons in **A** and **B** are therefore fixed and we deal with a single composition i.e. **AB**. In addition we assume that the projectile remains in it's ground state $\left|\psi_0^A\right\rangle$. The projectile-target state $\left|\psi_i^{AB}\right\rangle$ is then the product of the projectile ground state and the target excited states

$$\left|\psi_i^{AB}\right\rangle = \left|\psi_0^A\right\rangle \left|\psi_i^B\right\rangle \ . \tag{2.46}$$

Since the projectile remains in the ground state $\left|\psi_0^A\right\rangle$ the possible projectile-target states are uniquely identified by the target states $\left|\psi_i^B\right\rangle$. Hence we drop in the following the reference to **AB** and use the notation $|\psi_i\rangle$ for the excited states of the projectile-target system.

To derive the general optical potential we define the projection operator to the elastic channel $\mathcal{P} = |\Psi_0\rangle \langle\Psi_0|$ and its complement $\mathcal{Q} = \mathbf{1} - \mathcal{P}$ with the properties

$$\mathcal{P} + \mathcal{Q} = \mathbf{1} \ , \tag{2.47}$$
$$\mathcal{P}\mathcal{P} = \mathcal{P} \ , \tag{2.48}$$
$$\mathcal{Q}\mathcal{Q} = \mathcal{Q} \ , \tag{2.49}$$
$$\mathcal{Q}\mathcal{P} = \mathcal{P}\mathcal{Q} = 0 \ . \tag{2.50}$$

Inserting $\mathbf{1} = \mathcal{P} + \mathcal{Q}$ into the Schrödinger equation (2.37) and multiplying it from the left with the two projection operators yields

$$\left(E - \mathcal{P}\widehat{H}\mathcal{P}\right) \mathcal{P} \left|\Psi\right\rangle = \mathcal{P}\widehat{H}\mathcal{Q}\mathcal{Q} \left|\Psi\right\rangle \ , \tag{2.51}$$
$$\left(E - \mathcal{Q}\widehat{H}\mathcal{Q}\right) \mathcal{Q} \left|\Psi\right\rangle = \mathcal{Q}\widehat{H}\mathcal{P}\mathcal{P} \left|\Psi\right\rangle \ . \tag{2.52}$$

This is a coupled system of equations which couples the elastic channel to the inelastic ones. From Eq. (2.52) we obtain

$$\mathcal{Q}\left|\Psi\right\rangle = \frac{1}{E - \mathcal{Q}\widehat{H}\mathcal{Q}}\mathcal{Q}\widehat{H}\mathcal{P}\mathcal{P}\left|\Psi\right\rangle \ , \tag{2.53}$$

which inserted into Eq. (2.51) yields an effective Schrödinger equation for the elastic scattering problem

$$\left(E - \mathcal{P}\widehat{H}\mathcal{P} - \mathcal{P}\widehat{H}\mathcal{Q}\frac{1}{E - \mathcal{Q}\widehat{H}\mathcal{Q} + i\eta}\mathcal{Q}\widehat{H}\mathcal{P}\right)\mathcal{P}\left|\Psi\right\rangle = 0 \ . \tag{2.54}$$

The first interaction term $\mathcal{P}\widehat{H}\mathcal{P}$ is the so called direct term which is essentially the shell model contribution. The second interaction term describes the contributions due to coupling to inelastic channels. The coupling term can be interpreted as a three step process. First, due to the interaction there is a transition from $\left|\Psi_0\right\rangle$ to $\left|\Psi_i\right\rangle$. Then the projectile-target system propagates in the state $\left|\Psi_i\right\rangle$, which finally, couples back to $\left|\Psi_0\right\rangle$ via the interaction. The intermediate propagation is given by the Green function

$$G = \sum_{i,j\neq 0}\frac{\left|\Psi_i\right\rangle\left\langle\Psi_j\right|}{E - \mathcal{Q}\widehat{H}\mathcal{Q} + i\eta} \ . \tag{2.55}$$

We assume a weak coupling between the excited states

$$\left\langle\Psi_i\right|V\left|\Psi_i\right\rangle \gg \sum_{j\neq i}\left\langle\Psi_i\right|V\left|\Psi_j\right\rangle \ , \tag{2.56}$$

so that we can in first order replace the term $\mathcal{Q}\widehat{H}\mathcal{Q}$ by the expression $E-\epsilon_i-\widehat{T}_0+i\eta$ and the Green function becomes diagonal

$$G = \sum_{i\neq 0}\frac{\left|\Psi_i\right\rangle\left\langle\Psi_i\right|}{E - \epsilon_i - \frac{\hbar^2 k_i^2}{2\mu_i} + i\eta} \ . \tag{2.57}$$

We emphasize that the coupling between the channels is mutual for the whole calculation. Without the coupling between the channels the term $\mathcal{Q}\widehat{V}\mathcal{P}$ would vanish and no intermediate channel excitation would take place. With the assumption of Eq. (2.56) our results only represent the first order corrections to the optical potential.

We replace the wave function in Eq. (2.54) by the product $\left|\Psi_i\right\rangle = \left|\psi_i\right\rangle\left|k_i\right\rangle$ and make use of Eq. (2.41) to derive the general optical potential $V_{\rm opt}$ for the relative motion in the elastic channel

$$\left(\frac{\hbar^2 k_0^2}{2\mu_i} + V_{\rm opt}\right)\left|k_0\right\rangle = E\left|k_0\right\rangle \ , \tag{2.58}$$

with

$$V_{\rm opt} = \langle\psi_0| V |\psi_0\rangle + \sum_{i\neq 0} \langle\psi_0| V \frac{|\psi_i\rangle \langle\psi_i|}{E - \epsilon_i - \frac{\hbar^2 k_i^2}{2\mu_i} + i\eta} V |\psi_0\rangle \ . \tag{2.59}$$

The sum $i$ runs over all open channels except the elastic one. The optical potential has an imaginary part that accounts for the inelastic scattering, which becomes clear when we use the relation

$$\frac{1}{x + i\eta} = \frac{\mathbf{P}}{x} - i\pi \ \delta(x) \tag{2.60}$$

where $\mathbf{P}$ denotes the principal value. The imaginary part of the optical potential is then

$$\begin{aligned} \text{Im } V_{\rm opt} &= \text{Im } \sum_{i\neq 0} \langle\psi_0| V \frac{|\psi_i\rangle \langle\psi_i|}{E - \epsilon_i - \frac{\hbar^2 k_i^2}{2\mu_i} + i\eta} V |\psi_0\rangle & (2.61) \\ &= i\pi \sum_{i\neq 0} \langle\psi_0| V \ \delta(E - \epsilon_i - \frac{\hbar^2 k_i^2}{2\mu_i}) \ V |\psi_0\rangle & (2.62) \end{aligned}$$

This diploma thesis aims at the calculation of the imaginary part of the optical potential given by Eq. (2.61) and Eq. (2.62). We will evaluate Eq. (2.61) by explicitly calculating the transition densities for the intermediate states and their propagation with the Green function. The total imaginary part of the optical potential is then given as the sum of all open channel contributions.

## 2.4 The $\alpha$-nucleus optical potential

Based on the general optical potential given by Eq. (2.61) Villars [19] derived the exact optical potential in momentum space in second quantization

$$V_{\rm opt} = V_{HF} + \sum_{i\neq 0}^{N} S^{(i)}(k', k) \ , \tag{2.63}$$

with

$$\begin{aligned} &S^{(i)}(k', k) = \sum_{s+t+u=i} \\ &\left\langle 0 \left| \left(\frac{V}{E_0 - H_0}\right)^s J(k') \frac{1}{E - H_0 + i\eta} \left(V \frac{1}{E - H_0 + i\eta}\right)^t J^\dagger(k) \left(\frac{V}{E_0 - H_0}\right)^u \right| 0 \right\rangle_{\rm LC} \\ &- \left\langle 0 \left| \left(\frac{V}{E_0 - H_0}\right)^s J^\dagger(k) \frac{-1}{E - H_0 + i\eta} \left(V \frac{-1}{E - H_0 + i\eta}\right)^t J(k') \left(\frac{V}{E_0 - H_0}\right)^u \right| 0 \right\rangle_{\rm LC} , \end{aligned} \tag{2.64}$$

where the subscript LC shall indicate that only linked cluster graphs are taken into account. The energy $E_0$ is the energy of the unperturbed Hartree-Fock ground state $|0\rangle$ derived form the Hartree-Fock Hamiltonian $H_0$. The interaction operators are then

$$\begin{aligned} J(k) &= [c_k, V] = \sum_{\beta,\gamma,\delta} c^\dagger_\beta \langle k\beta \,|V|\, \gamma\delta\rangle \, c_\delta c_\gamma \ , \\ J^\dagger(k) &= \left[V, c^\dagger_k\right] = \sum_{\lambda,\mu,\nu} c^\dagger_\lambda c^\dagger_\mu \langle \lambda\mu \,|V|\, k\nu\rangle \, c_\nu \ . \end{aligned} \tag{2.65}$$

The independent sum over all powers $s$ and $u$ with the linked cluster restriction will produce the exact target ground state and the independent sum over $t$ reproduces the Green function between the two interaction operators $J^\dagger(k)$ and $J(k')$.

Osterfeld, Wambach and Madsen [3] then derived a general second order expression for the imaginary part of the optical potential including direct and exchange parts of the potential. The derivation is rather lengthy and is not given here. Dermawan, Osterfeld and Madsen[17] restricted the calculations from [3] to spinless $\alpha$-particles and gave the simplified expression for the imaginary part of the optical potential in $r$ space

$$W(\vec{r},\vec{r}') = \mathrm{Im} \sum_{i\neq 0}^{N} \langle 0 \,|V|\, \Psi_i\rangle_{\vec{r}} \, g_i(\vec{r},\vec{r}') \, \langle \Psi_i \,|V|\, 0\rangle_{\vec{r}} \ , \tag{2.66}$$

where $\langle \Psi_i \,|V|\, 0\rangle_{\vec{r}}$ gives the transition probability from the ground state $|\Psi_0\rangle$ to the intermediate state $|\Psi_i\rangle$ and $g_i(\vec{r},\vec{r}')$ is the Green function describing the motion of the projectile in the intermediate state. The Green function is calculated for the incident kinetic energy $E$ reduced by the excitation energy $\Delta\epsilon_{i,f}$ of the intermediate state. For $\alpha$-particles scattered by a spinless target nucleus ($J_A = 0^+$) the imaginary part of the optical potential than reads

$$W(\vec{r},\vec{r}') = \mathrm{Im} \left[ \frac{1}{16\pi^2} \sum_{\substack{l,l_c,L \\ J_N}} \delta_{L,J_N} \frac{\widehat{l}^2\widehat{l}_c^2}{\widehat{L}^2} \, (l0l_c0|L0) \ , F^D_{J_N,L0L}(r) g_{l_c}(r,r') F^D_{J_N,L0L}(r') P_l(\cos\theta) \right] , \tag{2.67}$$

with $\widehat{l} = \sqrt{2l+1}$ and the Legendre polynomials $P_l(\cos\theta)$.

The transition form factor $F^D_{J_N,L0L}(r)$ is given as the folding integral of the multipole expanded effective central $\alpha$-target interaction and the target nucleon density function.

$$F^D_{J_N,L0L}(r) = \int dr_1 r_1^2 \rho^{J_N}_{L0L}(r_1) v_L(r,r_1) \ . \tag{2.68}$$

The nucleon density function reads

$$\rho^{J_N}_{LSJ}(r) = \sum_{\substack{n_1 l_1 j_1 \\ n_2 l_2 j_2}} \left[X^{J_N}_{j_1,j_2} + Y^{J_N}_{j_1,j_2}\right] \frac{1}{\sqrt{4\pi}} \frac{\widehat{1}}{2} \widehat{S}\widehat{j_1}\widehat{j_2}\widehat{L}\widehat{J}\widehat{l_1} \times (l_1 0 L 0 | l_2 0) \left\{ \begin{array}{ccc} l_2 & \frac{1}{2} & j_2 \\ l_1 & \frac{1}{2} & j_1 \\ L & S & J \end{array} \right\} R_{n_1 l_1 j_1}(r) R_{n_2 l_2 j_2}(r) \ , \quad (2.69)$$

where $X^{J_N}_{j_1,j_2}$ and $Y^{J_N}_{j_1,j_2}$ are the RPA particle-hole amplitudes and $R_{n_i l_i j_i}$ are the radial single particle wave functions.

The derivation of the multipole expansion for the central alpha-target interaction is given in the appendix in Sec. A.3 and we repeat here only the result

$$v_l(r, r_1) = 2\pi \int_{-1}^{1} \mathrm{d}(\cos\theta)\ V(r') P_l(\cos\theta) \ , \quad (2.70)$$

$$r' = \sqrt{r^2 + r_1^2 - 2r\ r_1 \cos\theta} \ . \quad (2.71)$$

From Eq. (2.66)-(2.70) we can calculate the imaginary optical potential for spin 0 nuclei and consequently the reaction cross section $\sigma_\mathrm{r}$. For non magic nuclei with unpaired spin the more general expression from [3] has to be evaluated.

# Part II

# Implementation and Results

# Chapter 3

# Implementation

The aim of this work was to implement equations (2.66)-(2.70) as a computer code and to obtain results comparable to those from Osterfeld et. al. [17]. For the description of the excited states of the target, the particle-hole RPA amplitudes from S. Krewald and J. Speth[20] and R. Kogler [12] are used.

The following sections give the details about the implementation of the imaginary $\alpha$-$^{16}$O optical potential.

## 3.1 The Intermediate Potential

For the real part of the $\alpha$-$^{16}$O optical potential the double folding potential of a density dependent M3Y [21] interaction was chosen

$$U(\vec{r}) = \int \mathrm{d}^3\vec{r}_1 \int \mathrm{d}^3\vec{r}_2 \; \rho_T(\vec{r}_1) \; \rho_\alpha(\vec{r}_2) \; t(E, \rho_T, \rho_\alpha, \vec{s}) \; , \tag{3.1}$$

with the nucleon density functions $\rho_T$ and $\rho_\alpha$ for the target nucleus and the $\alpha$-particle. The effective M3Y nucleon-nucleon interaction $t$ is a function of the distance $\vec{s} = \vec{r} + \vec{r}_2 - \vec{r}_1$ between nucleons in the $\alpha$-particle and the target nucleus.

The effective density dependent M3Y nucleon-nucleon interaction is of the form

$$t(E, \rho_T, \rho_\alpha, \vec{s}) = \lambda \; g(E, \vec{s}) \; f(E, \rho) \; , \tag{3.2}$$

where $g(E, \vec{s})$ is the usual M3Y force modulated with a density dependent factor $f(E, \rho)$. The scaling factor $\lambda = 1.32$ is used to fit the total $\alpha$-$^{16}$O interaction to the experimental cross section data and was chosen according Ref. [22] and [23]. The M3Y interaction is

$$g(E, \vec{s}) = \left[ 7999 \frac{e^{-4s}}{4s} - 2134 \frac{e^{-2.5s}}{2.5s} \right] + \hat{J}_{00}(E) \; \delta(\vec{s}) \; , \tag{3.3}$$

where $\hat{J}_{00}$ accounts for the single-nucleon knock-on exchange,

$$\hat{J}_{00}(E) = -276(1 - 0.005 \frac{E}{A_\alpha}) \; , \tag{3.4}$$

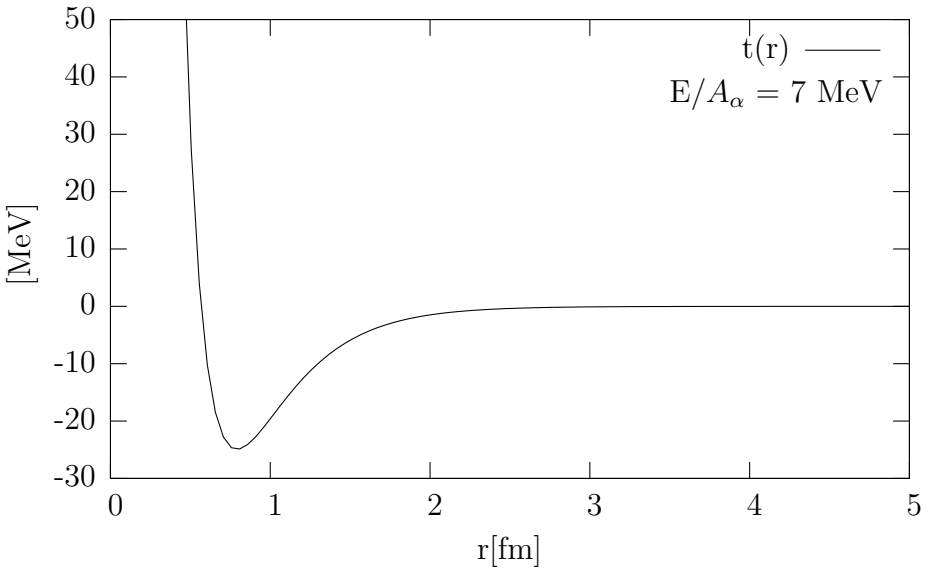


Figure 3.1: M3Y nucleon-nucleon interaction for two delta distributed nucleons

| $\frac{E}{A_\alpha}$ (MeV) | 7 | 10 | 15 | 20 | 25 | 29.5 | 35 |
|---|---|---|---|---|---|---|---|
| $\hat{J}_{00}$ (MeV fm$^3$) | -265.6 | -262.2 | -255.2 | -248.4 | -241.5 | -234.6 | -227.7 |
| $C$ | 0.444 | 0.420 | 0.405 | 0.380 | 0.354 | 0.336 | 0.279 |
| $\alpha$ | 4.10 | 4.24 | 4.21 | 4.25 | 4.37 | 4.39 | 5.14 |
| $\beta$ (fm$^3$) | 10.67 | 10.15 | 9.66 | 9.12 | 8.54 | 8.05 | 7.20 |

Table 3.1: Parameter for the density dependent M3Y interaction taken from [22]

with the projectile nucleon number $A_\alpha$. Following [22] the density dependent function $f(E, \rho)$ is of exponential form

$$f(E, \rho) = C(E) \left[1 + \alpha(E)\ e^{-\beta(E)\rho(\vec{r}_1, \vec{r}_2)}\right] \tag{3.5}$$

with the projetile-target density distribution

$$\rho(\vec{r}_1, \vec{r}_2) = \rho_T(\vec{r}_1) + \rho_\alpha(\vec{r}_2)\ . \tag{3.6}$$

The parameter $\hat{J}_{00}(E)$, $C(E)$, $\alpha(E)$ and $\beta(E)$ where taken from [22] and are listed in Tab. 3.1. A spline interpolation was used to derive the M3Y potential parameters for energies not given in Tab. 3.1. Fig. 3.1 shows the M3Y interaction given by Eq. (3.2) for two delta distributed nucleons at 7 MeV/A. The attractive potential has its minimum at 0.8 fm and shows a strong repulsive behavior below 0.5 fm.

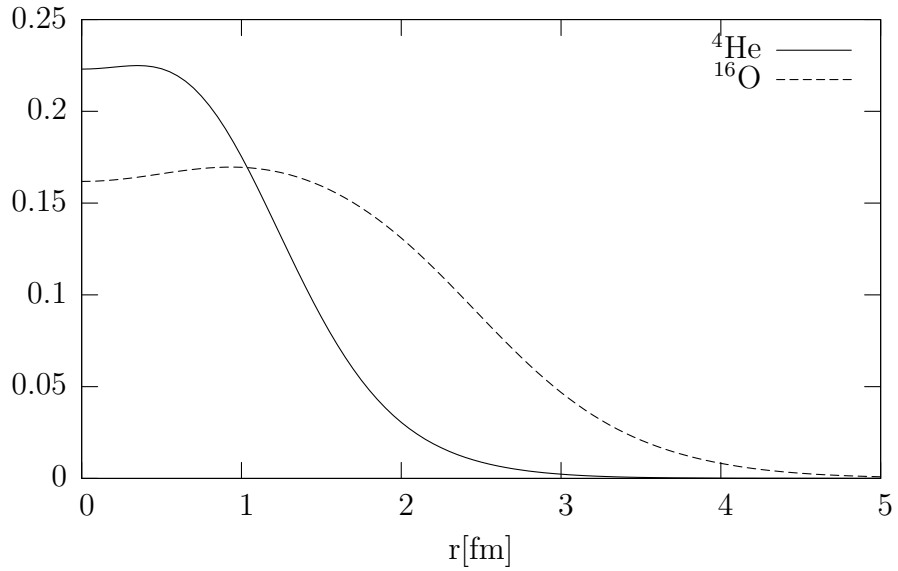


Figure 3.2: $^4$He and $^{16}$O nucleon densities

The nucleon density distribution is assumed to be proportional to the charge distribution [24]. The nucleon density is described by the sum of Gaussians

$$\rho(r) = \sum_i A_i \left[ e^{-\left(\frac{r-R_i}{\gamma}\right)^2} + e^{-\left(\frac{r+R_i}{\gamma}\right)^2} \right] , \tag{3.7}$$

with the amplitudes

$$A_i = \frac{N\ Q_i}{2\pi^{\frac{3}{2}}\gamma^3 \left(1 + \frac{2R_i^2}{\gamma^2}\right)} . \tag{3.8}$$

The parameters $R_i$, $Q_i$ and $\gamma$ determine the amplitude and the width of the $i^{\text{th}}$ Gaussian distribution and thus the radial shape of the nucleon density. In addition a normalization applies to the parameters $Q_i$

$$\sum_i Q_i = 1, \tag{3.9}$$

so that the nucleon density is normalized to the nucleon number $N$,

$$\int_0^\infty \mathrm{d}r\ r^2\ 4\pi\ \rho(r) = N\ . \tag{3.10}$$

The charge density parameters for $^4$He and $^{16}$O from [24] are given in Tab. 3.1 and Fig. 3.2 shows the corresponding nucleon-densities.

The effective $\alpha$-target interaction is the double folding integral from the nucleon density distributions $\rho_\alpha$, $\rho_T$ and the effective density dependent nucleon-

| | $^4$He | | $^{16}$O | |
|---|---|---|---|---|
| $\gamma$ | 0.8615 | | 1.0614 | |
| i | $R_i$ | $Q_i$ | $R_i$ | $Q_i$ |
| 1 | 0.2 | 0.034724 | 0.4 | 0.057056 |
| 2 | 0.6 | 0.430761 | 1.1 | 0.195701 |
| 3 | 0.9 | 0.203166 | 1.9 | 0.311188 |
| 4 | 1.4 | 0.192986 | 2.2 | 0.224321 |
| 5 | 1.9 | 0.083866 | 2.7 | 0.059946 |
| 6 | 2.3 | 0.033007 | 3.3 | 0.134714 |
| 7 | 2.6 | 0.014201 | 4.1 | 0.000024 |
| 8 | 3.1 | 0.000000 | 4.6 | 0.013961 |
| 9 | 3.5 | 0.006860 | 5.3 | 0.000007 |
| 10 | 4.2 | 0.000000 | 5.6 | 0.000002 |
| 11 | 4.9 | 0.000438 | 5.9 | 0.002096 |
| 12 | 5.2 | 0.000000 | 6.4 | 0.000002 |

Table 3.2: Parameter for the nucleon density distribution given by [24]

nucleon interaction of Eq. (3.2),

$$\begin{aligned} U(\vec{r}) &= \lambda\, C \left[ \int \mathrm{d}^3\vec{r}_1 \int \mathrm{d}^3\vec{r}_2\ \rho_T(\vec{r}_1)\ \rho_\alpha(\vec{r}_2)\ g(\vec{s}) \right. \\ &+ \left. \alpha \int \mathrm{d}^3\vec{r}_1 \int \mathrm{d}^3\vec{r}_2\ \rho_T(\vec{r}_1) e^{-\beta\rho_T(\vec{r}_2)}\ \rho_\alpha(\vec{r}_2) e^{-\beta\rho_\alpha(\vec{r}_2)}\ g(\vec{s}) \right] . \end{aligned} \tag{3.11}$$

The numerical evaluation of the double folding integral Eq. (3.11) is most efficiently performed via Fourier transformation techniques.[1]

$$U(r) = \lambda C (2\pi)^3 \mathrm{Ft}\Big[ \mathrm{Ft}[g] \left( \mathrm{Ft}[\rho_T]\mathrm{Ft}[\rho_\alpha] + \alpha \mathrm{Ft}[\rho_T e^{-\beta\rho_T}]\mathrm{Ft}[\rho_\alpha e^{-\beta\rho_\alpha}] \right) \Big] \tag{3.12}$$

with

$$\mathrm{Ft}[f] = \frac{2}{(2\pi)^{\frac{1}{2}}} \int_0^\infty \mathrm{d}r\ r^2 f(r) \frac{\sin(kr)}{kr} , \tag{3.13}$$

where $\mathrm{Ft}[f]$ is the 3 dimensional Fourier transform of the function $f(r)$. For the M3Y interaction from Eq. (3.3) the Fourier transformation can be calculated in closed form

$$\mathrm{Ft}(g) = \frac{2}{(2\pi)^{\frac{1}{2}}} \left( \frac{7999}{4(4^2+k^2)} - \frac{2134}{2.5(2.5^2+k^2)} \right) + \frac{\hat{J}_{00}}{(2\pi)^{\frac{3}{2}}} . \tag{3.14}$$

## 3.2 The Green Function

The Green function for the propagation in the intermediate state is calculated from the effective $\alpha$-$^{16}$O interaction potential shown in Fig. 3.3. The energy $E_{\mathrm{int}}$ in the intermediate channel is the incident energy $E$ reduced by the excitation energy $\Delta\epsilon_{i,f}$ of the single particle-hole state

$$E_{\mathrm{int}} = E - \Delta\epsilon_{i,f} . \tag{3.15}$$

Therefore the Green function $G(\vec{r},\vec{r}')$ satisfies

$$\left( \widehat{H}(\vec{r}) - E_{\mathrm{int}} \right) G(\vec{r},\vec{r}') = \delta^3(\vec{r},\vec{r}') \tag{3.16}$$

with the Hamilton operator $\widehat{H}(\vec{r})$ for the $\alpha$-$^{16}$O interaction potential $U(r)$

$$\widehat{H}(\vec{r}) = -\frac{\hbar^2}{2\mu} \left( \frac{1}{r} \frac{\mathrm{d}^2}{\mathrm{d}r^2} r - \frac{\widehat{L}^2}{r^2} \right) + U(r) . \tag{3.17}$$

[1] The derivation of Eq. (3.12) is given in the appendix Sec. A.1

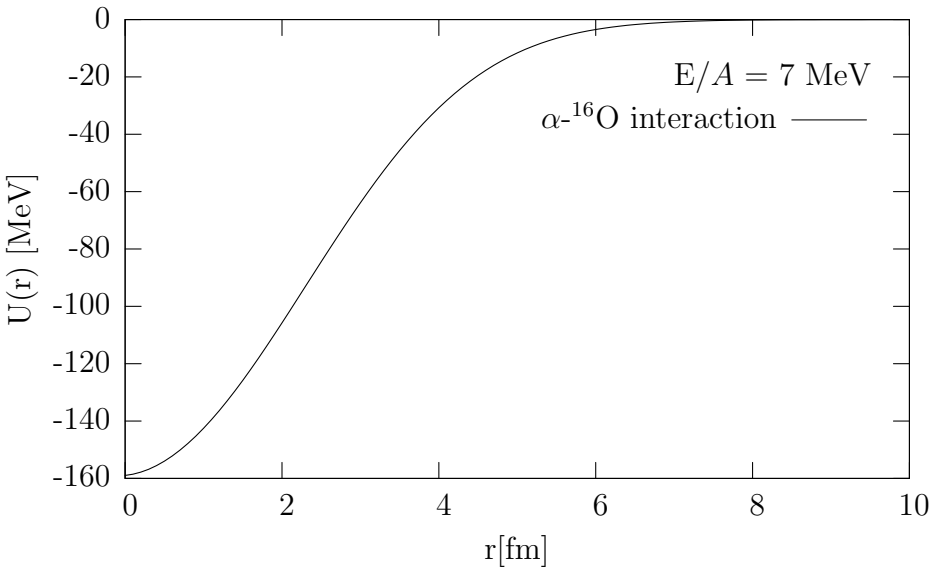


Figure 3.3: $\alpha$ - $^{16}$O interaction potential

Here $\mu$ is the reduced mass of the $\alpha$ particle and $\widehat{L}$ is the angular momentum operator. For a compact notation we have not explicitly written the energy dependence of the $\alpha$-$^{16}$O interaction potential $U(r)$. The Green function is calculated with the actual potential for each intermediate channel separately.

The expansion of the Green function in spherical harmonics reads

$$\begin{aligned} G(\vec{r},\vec{r}') &= \sum_{l=0}^{\infty} G_l(r,r') \sum_{m=-l}^{l} Y_{lm}(\hat{r}) Y_{lm}(\hat{r}') \\ &= \sum_{l=0}^{\infty} G_l(r,r') \frac{2l+1}{4\pi} P_l(\cos\theta) \ , \end{aligned} \tag{3.18}$$

where $G_l(r,r')$ are the radial Green functions for the angular momentum $l$. For the three dimensional delta function $\delta^3(\vec{r})$ we use the expression,

$$\begin{aligned} \delta^3(\vec{r},\vec{r}') &= \frac{1}{rr'}\delta(r-r') \sum_{l=0}^{\infty} \sum_{m=-l}^{l} Y_{lm}(\hat{r}) Y_{lm}(\hat{r}') \\ &= \frac{1}{rr'}\delta(r-r') \sum_{l=0}^{\infty} \frac{2l+1}{4\pi} P_l(\cos\theta) \ . \end{aligned} \tag{3.19}$$

Inserting Eq. (3.18) and Eq. (3.19) into the Schrödinger equation (3.16) one obtains the equation for the radial Green functions $G_l(r,r')$

$$\left( -\frac{\hbar^2}{2\mu} \left[ \frac{1}{r} \frac{\mathrm{d}^2}{\mathrm{d}r^2} r - \frac{l(l+1)}{r^2} \right] + V(r) - E_{\mathrm{int}} \right) G_l(r,r') = \frac{1}{rr'}\delta(r-r') \ . \tag{3.20}$$

| E | $V_1$ | $\alpha$ | $V_2$ | $\alpha$ |
|---|---|---|---|---|
| 30 | -310.1 | 0.422 | 319.2 | 0.505 |
| 100 | -387.6 | 0.422 | 398.9 | 0.505 |

Table 3.3: Effective $\alpha$-nucleon interaction parameter

The radial Green function $G_l(r, r')$ is constructed as the product of the regular $\phi_l(r)$ and the irregular $\psi_l(r)$ solutions from the homogeneous Schrödinger equation

$$\left(-\frac{\hbar^2}{2\mu}\left[\frac{1}{r}\frac{\mathrm{d}^2}{\mathrm{d}r^2}r - \frac{l(l+1)}{r^2}\right] + V(r) - E_{\mathrm{int}}\right)\phi_l(r) = 0 \ . \tag{3.21}$$

The radial Green function is given by

$$G_l(r, r') = N_l g_l(r, r') \tag{3.22}$$

$$g_l(r, r') = -\frac{1}{k}\phi_l(r_<)\psi_l(r_>) \ , \tag{3.23}$$

where $r_<$ is the smaller and $r_>$ the bigger value of the two radii $r$ and $r'$. The wave vector $k$ is evaluated for the intermediate state with $k = \sqrt{2\mu E_{\mathrm{int}}/\hbar^2}$ and $N_l$ is a complex constant[2]

$$N_l = -\frac{2\mu}{\hbar^2}\frac{k}{r'^2}\left(\phi_l(r')\left.\frac{\mathrm{d}}{\mathrm{d}r}\psi_l(r)\right|_{r'} - \psi_l(r')\left.\frac{\mathrm{d}}{\mathrm{d}r}\phi_l(r)\right|_{r'}\right)^{-1} \ . \tag{3.24}$$

Fig. 3.4 shows the Green function calculated from the $\alpha$-$^{16}$O nucleus-nucleus interaction for $\cos\theta = 1$. We see that the Green function is peaked along the diagonal $r = r'$ and shows oscillations perpendicular to the diagonal. With rising energy the peak becomes more pronounced with shorter wave length of the oscillations perpendicular to the diagonal. In addition the Green function in Fig. 3.4 shows a characteristic rise at small radii due to the $\alpha$-$^{16}$O interaction.

## 3.3 Transition form factor

For the $\alpha$-nucleon interaction in the transition form factor we choose a phenomenological potential of Gaussian shape

$$V(r) = V_1\ e^{-\alpha r^2} + V_2\ e^{-\beta r^2} \ . \tag{3.25}$$

The parameters of the phenomenological $\alpha$-nucleon potential are given in Tab. 3.3.

Fig. 3.5 shows the $\alpha$-nucleon interaction for 30 MeV and 100 MeV. It is obvious that the effective energy dependence of the potential is rather small. The

[2]The derivation of Eq. (3.24) is given in the appendix Sec. A.2.

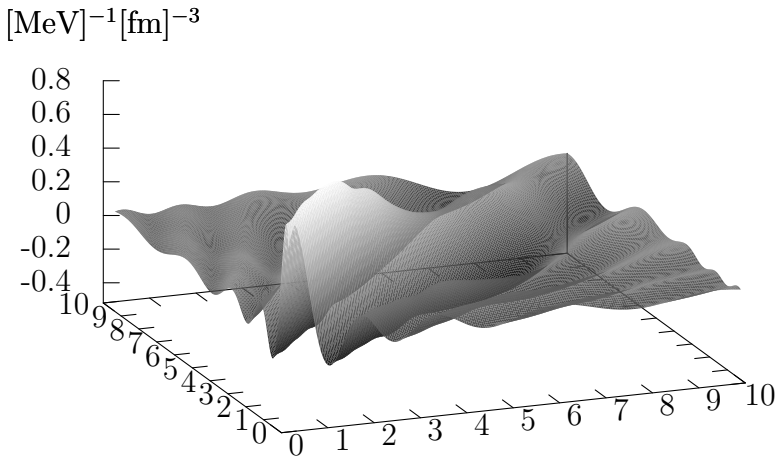


Figure 3.4: Imaginary part of the optical Green function at $E = 21$MeV for the $\alpha$-$^{16}$O interaction potential of Fig. 3.3 and $\cos\theta = 1$

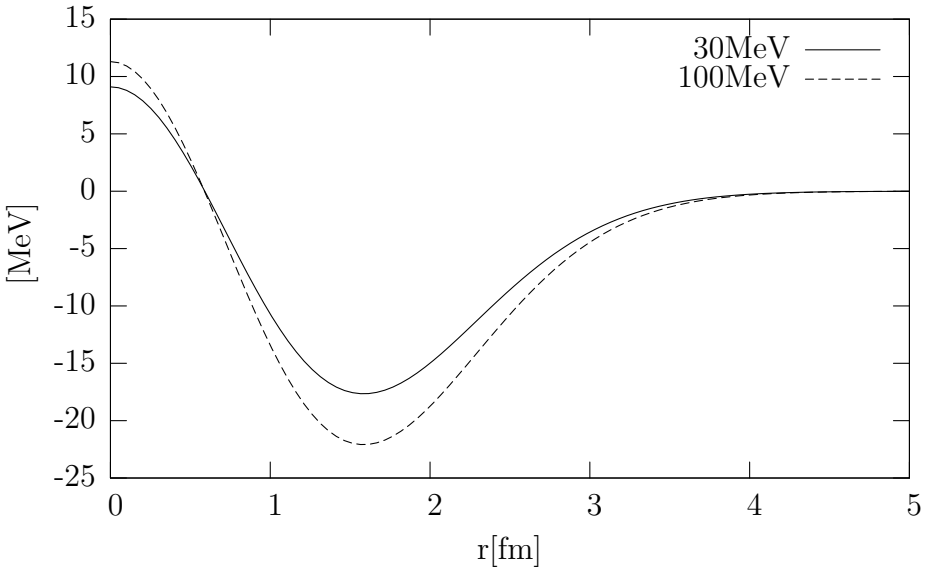


Figure 3.5: Effective $\alpha$-nucleon potential for 30MeV and 100 MeV

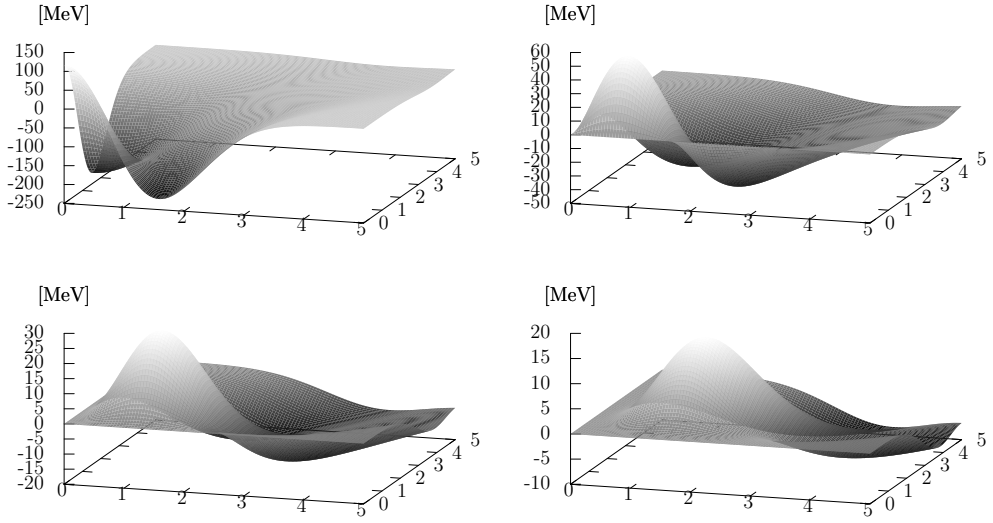


Figure 3.6: Multipole expansion of the effective $\alpha$-nucleon potential for the angular momentum l=0 (top left), l=1 (top right) l=2 (bottom left) and l=3 (bottom right)

main scope of this diploma thesis is the $\alpha$-$^{16}$O optical potential at low energies. Therefore we use in our calculations the parameters for 30 MeV. From the multipole expansion shown in Fig. 3.6 we see that for a given partial wave the radial potentials $v_l(r, r')$ are peaked along the diagonal $r = r'$. For higher $l$ values the height of the peak decreases and is shifted towards higher $r$-values.

To obtain the transition form factor $F^D_{J_N,L0L}(r)$ the $\alpha$-nucleon interaction was folded with the nucleon density function which was calculated from the RPA particle-hole amplitudes[3][20]. Fig. 3.7 and Fig. 3.8 show the resulting nucleon density functions and the transition form factors for the three lowest lying $3^-$ states in $^{16}$O.

Fig. 3.8 shows that the biggest contributions come from the states at 6.5 MeV and 47.0 MeV. The state with the excitation energy of 18.9 MeV has a very small contribution as the RPA amplitudes for the $T = 0$ and $T = 1$ particle-hole amplitudes almost compensate each other. We further see that the transition form factor of the 6.5 MeV state is dominated by the 1p $\rightarrow$ 1d transition and thus peaked at a slightly smaller radius than the 1p $\rightarrow$ 1g dominated 47.0 MeV state.

[3]The RPA single particle-hole excitation amplitudes from [20] are given in the appendix in Sec. B.1.

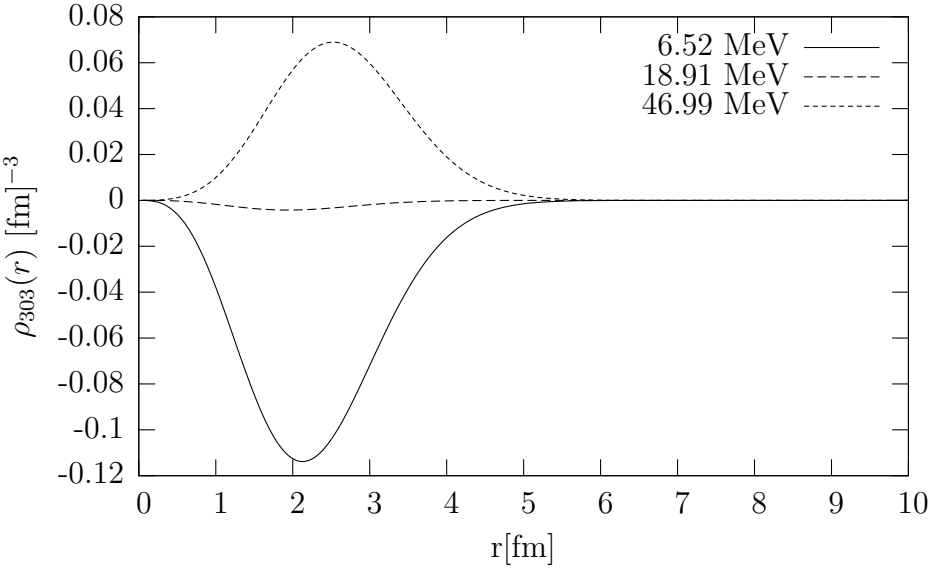


Figure 3.7: RPA density function for the 3 lowest lying $3^-$ states of the $^{16}$O System [20]

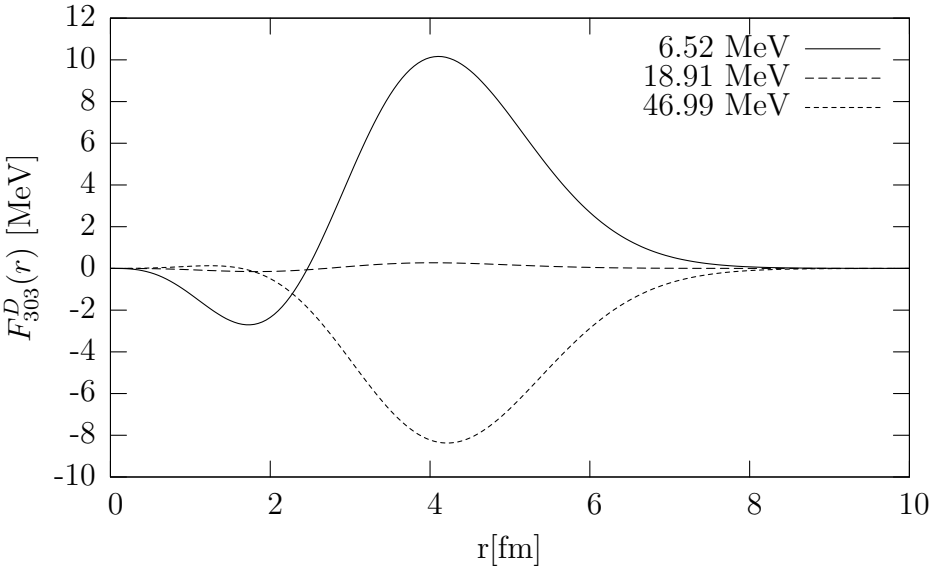


Figure 3.8: Transition form factors for the 3 lowest lying $3^-$ states of $^{16}$O obtained from the nucleon density functions of Fig.3.7 and the effective $\alpha$-nucleon interaction of Fig. 3.5

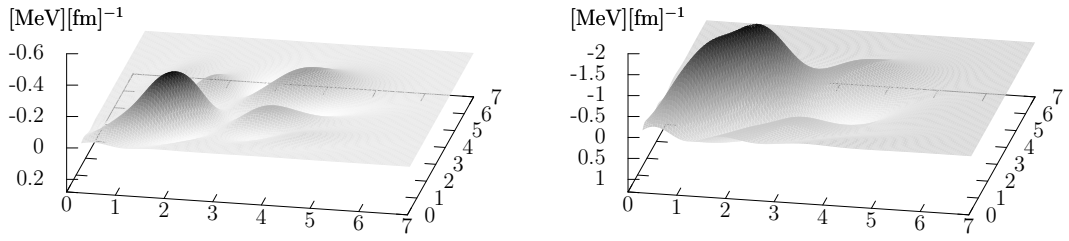


Figure 3.9: Imaginary $\alpha$-$^{16}$O potential at 18 MeV (left) and at 30 MeV (right)

## 3.4 Results

According to Eq. (2.66) the imaginary $\alpha$-$^{16}$O optical potential arises from the contributions of all open channels for the incident $\alpha$-particle energy $E$.

When we compare the imaginary $\alpha$-$^{16}$O optical potential at 30 MeV, shown in Fig. 3.9, with the results given by F. Osterfeld, J.Wambach and V.A. Madsen [3] for the $\alpha$-$^{40}$Ca potential we see that we reproduce the overall form but not the absolute size. This difference can be explained with the bigger number of open channels in $^{40}$Ca than in $^{16}$O.

Fig. 3.10 shows that the main contribution to the optical potential at 30 MeV comes from the $1^-$ and $3^-$ states. At 30 MeV the $3^-$ contribution to the optical potential is about 5 MeV according to Osterfeld et.al. while our calculations show only a contribution of 0.2 MeV. When looking at the RPA calculations for the $3^-$ states we see that for $^{40}$Ca V. Gillet and E.A. Sanderson [25] obtained 18 states below 20 MeV while the $^{16}$O calculation from Speth and Krewald [20] contain only 2 states. From the higher number of open channels in $^{40}$Ca it is understandable that the absolute value of the imaginary optical potential is also bigger in $^{40}$Ca.

We tried to compare our results with nuclear cross section measurements, which turned out very difficult as no experimental data set for non-elastic cross sections is available below 70 MeV. To calculate the imaginary optical potential for energies above 70 MeV we would need much more involved RPA calculations taking a bigger number of particle-hole excitations as well as the continuum into account. Those calculations are not available and thus we tried a different approach.

The imaginary part of the optical potential accounts for the loss of flux in the elastic channel thus we tried to compare the absolute values of the differential elastic cross section measurements with the values obtained from our potential. The comparison turned out to be very difficult, as the real part of our $\alpha$-$^{16}$O optical potential does not reproduce the angular distribution of the scattering data and thus the comparison of the absolute values was not possible. Fig.

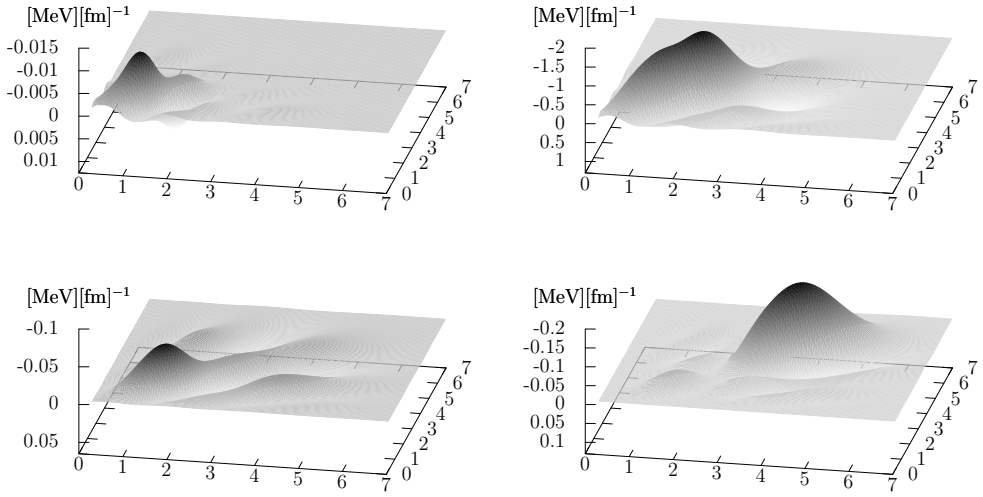


Figure 3.10: Contributions to the $\alpha$-$^{16}$O optical potential from the $0^+$ (top left), the $1^-$ (top right), the $2^+$ (bottom left) and $3^-$ (bottom right) states at 30 MeV

3.11 shows the differential elastic cross section obtained from our results with the experimental data from J.C. Corelli et al.[26] at 18 MeV. We used a scaling factor $\lambda$ for the imaginary part of the potential and plotted the results for $\lambda = 0, 1$ and 10.

For the real part the double folding potential was used. Unfortunately the angular distribution of the differential elastic cross section is not reproduced sufficiently well by the total optical potential. Nevertheless the almost negligible effect of the imaginary part is clearly seen. For a better reproduction of the experimental results it is therefore most important to determine a realistic real part of the $\alpha$-$^{16}$O optical potential first.

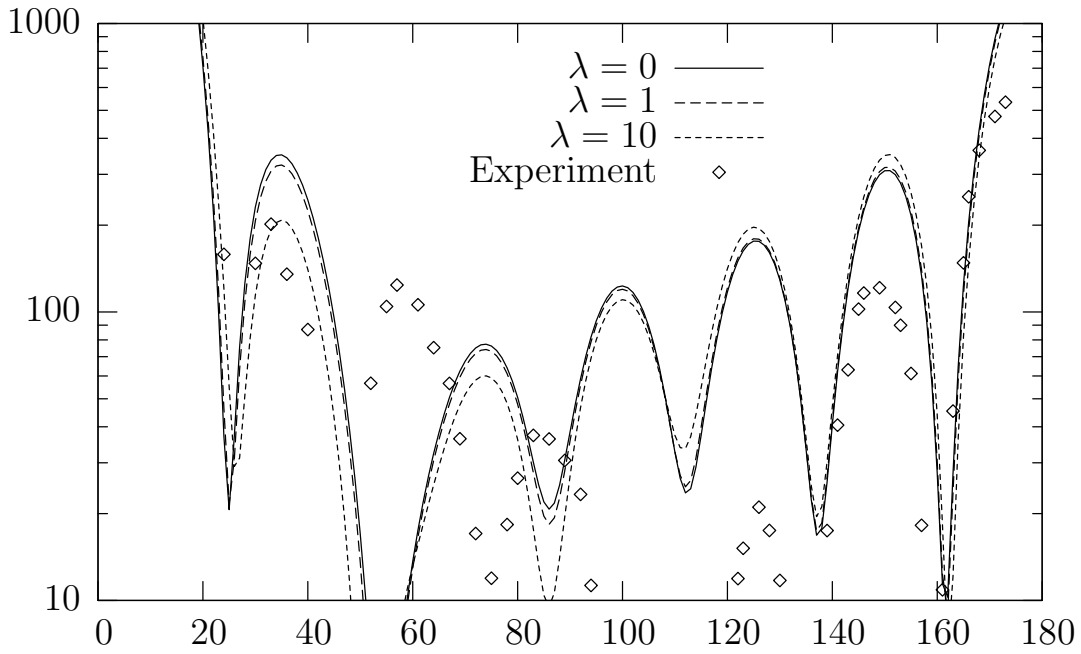


Figure 3.11: Calculated and experimental[26] differential elastic cross section data of the $\alpha$-$^{16}$O system at 18MeV

# Part III

# Program and Source Code

# Chapter 4

# The source code

The software was implemented on a Linux system and the GNU g95 Fortran compiler. Beside the standard g95 library options `-lm` and `-lg2c` the open source libraries `-lkernlib` and `-lmathlib` from the cernlib[1] are required to compile the code.

The software itself is written in a modular way which allows to easily reuse parts and to replace certain modules like e.g. the $\alpha$-$^{16}$O interaction potentials. The layout of the software is depicted in Fig. 4.1. The software is controlled through a configuration file which allows to change the calculation parameter and to include easily different RPA amplitudes or potentials without recompiling the software.

## 4.1 General Description

As shown in Fig. 4.1 the program consist of 3 global configuration and support files which read the configuration data and provide general definitions of data types, constants and functions that are used throughout all modules. Whereas `config.f95` reads the configuration file, `nrtype.f95` is used to define constants and data types and `support.f95` supplies common routines like Simpson integration or the shooting method to calculate the solutions of the Schrödinger equation.

`alnucpot.f95` calculates the $\alpha$-nucleon potential between the $\alpha$-particle and the RPA nucleon states. The RPA single particle-hole amplitudes are read by `rpaAmps.f95` and used to calculate the nuclear density function $\rho^{J_N}_{LSJ}$ in the module `rho.f95`. The transition form factor $F^D_{J_N,L0L}(r)$ is calculated in `formfact.f95`

[1]The cernlib my be obtained from `http://cernlib.web.cern.ch/cernlib/` or as a binary packages from your Linux distribution. To compile the cernlib from source it might be necessary to also install the LAPACK library which is available from `http://www.netlib.org/lapack/lug/lapack_lug.html` and the BLAS library available at `http://www.netlib.org/blas/index.html`

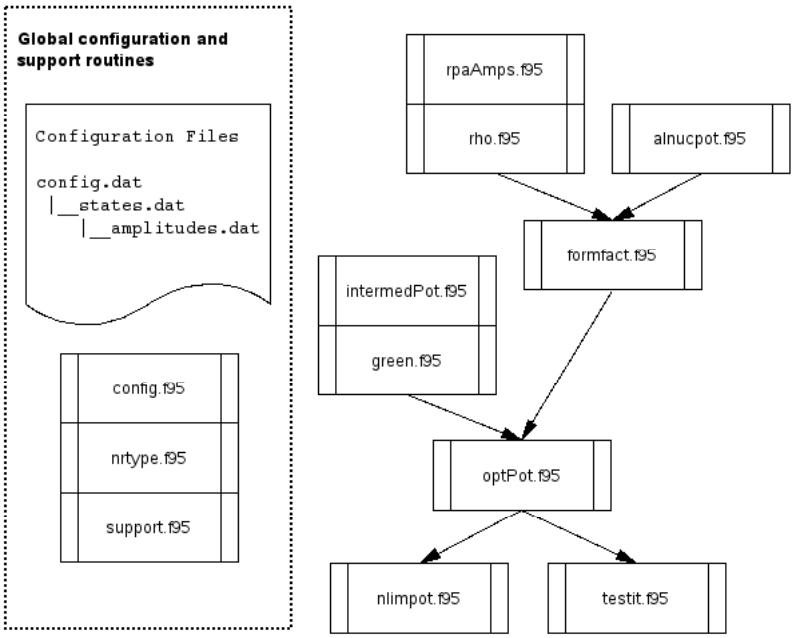


Figure 4.1: Module overview

and is combined to the optical potential in `optPot.f95`. The Green function therefore is calculated in the module `green.f95` from the regular and irregular solution for the intermediate potential which is calculated by `intermedPot.f95`.

To speed up the calculation most modules are designed to receive a call to a `calc` procedure that calculates the desired function values and stores the result in an internal data structure. The results can than be obtained by consecutive calls to the `get` function. The dimensions of the data structures in the memory are fixed. The internal storage size and the sampling distance are chosen to hold the data with sufficient accuracy up to a cutoff radius. Typically the cutoff radius is 10 fm such that the contributions from values above the cutoff radius are negligible.

`nlimpot.f95` is the main program which includes the modules and has a main loop to calculate the nonlocal imaginary potential. The program `testit.f95` contains a set of test routines that can be used to printout intermediate results of the modules for debugging purposes and was used to prepare the figures of this thesis.

The routines itself are documented within the source code. To ease the debugging and reuse of the code the following programming conventions where used.

- Variables names are chosen with self explaining names in lower case.
- Configuration variables and constants are UPPER case.

- All modules use implicit variable declaration to ensure that all variables have proper types.
- Global variables where avoided if possible.
- The function names are usually composed from several words where all words start with a capital letter except the first. (e.g. `readConfigFile`)

The following section will give a short description of the modules, their initialization, dependencies, the file formats used and the available options to test the modules.

## 4.2 config.f95

The configuration of the program is read from the configuration file. The name of the configuration file is specified in the call of `readConfigFile(filename)`. The configuration file uses a `name = value` syntax. The `#` indicates a comment. All characters following the `#` are discarded. The module defines default values for all configuration options except the filename of the RPA amplitudes.

The main configuration options are given in Tab. 4.2 the remaining options for the testing of the modules are given with the module description.

## 4.3 rpaAmps.f95

The module `rpaAmps.f95` reads the RPA amplitudes $X^{J_N}_{j_1,j_2}$ and $Y^{J_N}_{j_1,j_2}$. The routine allocates dynamically the memory required to store the amplitudes.

### Initialization

To initialize the module call `rpaInit(filename)` with the filename that contains the RPA amplitudes. To avoid error messages about improper memory management the function `rpaFree()` should be called when the calculations are finished.

### Fileformat

The configuration of the module is managed by two configuration files. The name of the main configuration file is given to `rpaInit(filename)` which contains aside from the description of the particle hole states the filename of the second RPA file .

The syntax of the configuration files is fixed. It is variable only to the extent that the number of lines for the particle and hole states can change. The data

| Name | Type | Def. | Description |
|---|---|---|---|
| DEBUG_LEVEL | int | −1 | Sets the debug level of the program. 0 and below indicates no debug information. 1 prints moderate and 2 detailed debug information to the screen while executing the program. |
| RPA_FILENAME | char[40] | | specifies the filename from which the RPA amplitudes should be read. |
| PROJECTILE_N | int | 4 | Specifies the number of nucleons in the target and the projectile |
| TARGET_N | int | 16 | |
| INCIDENT_ENERGY | real | 30.0 | Incident energy in the laboratory system for which the optical potential will be calculated. |
| GREEN_POT | int | 0 | Defines the intermediate potential for the Green function. 0 gives the free particle Green function and 1 uses a Gaussian folding potential. |
| MAX_L | int | 10 | Maximum angular momentum that is taken into account in the calculations. The parameter effects the effective interaction and the Green function. |
| COS_THETA | int | 0 | angle between $r$ and $r'$ for which the optical potential is calculated. |
| JN_CONTRIBUTE | int | −1 | Restricts the contributions of the RPA amplitude to a certain total angular momentum. When set to −1 all contributions are taken into account. |

Table 4.1: Main configuration file options

in each line may be followed by an arbitrary comment that has to be separated from the data by at least one blank character.

The first configuration file starts with the file name of the second configuration file followed by the number of hole states in the second line. The following two lines are a comment to make the configuration file better readable. Then for each of the hole states one line has to be given that contains the quantum numbers n, l, s, j and t. After a blank line the number of particle states is given and again 2 lines of comment followed by the table of particle state quantum numbers. A typical main configuration file for $^{16}$O would read

```
------ Begin: states.dat ------
amplitudes.dat                          # RPA amplitudes filename
3                                       # nbr of holes
# hole states
# n     l       s       j       t
1.      0.      0.5     0.5     0.5     # 1s_1/2
1.      1.      0.5     1.5     0.5     # 1p_3/2
1.      1.      0.5     0.5     0.5     # 1p_1/2

7                                       # nbr of particles
# particle states
# n     l       s       j       t
1.      2.      0.5     2.5     0.5     # 1d_5/2
2.      0.      0.5     0.5     0.5     # 2s_1/2
1.      2.      0.5     1.5     0.5     # 1d_3/2
1.      3.      0.5     3.5     0.5     # 1f_7/2
2.      1.      0.5     1.5     0.5     # 2p_3/2
1.      3.      0.5     2.5     0.5     # 1f_5/2
2.      1.      0.5     0.5     0.5     # 2p_1/2
------- End: states.dat -------
```

The RPA amplitudes for the RPA states are read from the second file which may contain an arbitrary number of data sets. Each data set is characterized by a line starting with `$` in the first column. The `$` has to be followed by 4 real numbers for the channel parameter: total angular momentum (J), isospin (T), parity (P) and the energy (E). The next line contains the RPA $X^{J_N}_{j_1,j_2}$ values followed by one line for the $Y^{J_N}_{j_1,j_2}$ values. Each line of amplitudes contain $n_p * n_h$ data entries where $n_h$ is the number of holes and $n_p$ the number of particles. The order of the entries is: $h_1$-$p_1$ $h_1$-$p_2$ $\ldots$ $h_1$-$p_{n_p}$ $h_2$-$p_1$ $\ldots$ $h_2$-$p_{n_p}$ $\ldots$ $h_{n_h}$-$p_{n_p}$.

Before and after each data set additional lines of comments may be inserted as long as they do not contain the `$` as their first character. A typical amplitude file looks like the following example where due to limited space only the first few data values are shown.

```
------ Begin: amplitudes.dat ------
!!!  RPA Amplitueds from S. Krewald and J. Speth
***** The used constants of this calculation are: ******
!!!
!!! S. Krewald and J. Speth. Phys. Lett. 52B. 295 (1974)
!!!
!!! J T P E
*******************************************************
$  3  1  0   6.52
  0.000  0.000  0.000 -0.124  0.110  0.000  0.000  0.000  ...
  0.003  0.001  0.000  0.007  0.000  0.000  0.000  0.000  ...
$  3  1  0  18.91
  0.000  0.000  0.000  0.000 -0.002  0.000  0.000  0.000  ...
  0.003  0.001  0.000  0.019  0.000  0.000  0.000  0.000  ...
------- End: amplitudes.dat -------
```

**Testing**

With the configuration option `WRITE_RPA_AMPS = 1` the RPA amplitudes will be written to the file `deb_rpaAmps.txt` which can be used to verify that the amplitudes where read properly.

## 4.4 rho.f95

The module `rho.f95` calculates the density function $\rho^{J_N}_{LSJ}(r)$ given by

$$\rho^{J_N}_{LSJ}(r) = \sum_{\substack{n_1 l_1 j_1 \\ n_2 l_2 j_2}} \left[X^{J_N}_{j_1,j_2} + Y^{J_N}_{j_1,j_2}\right] \frac{1}{\sqrt{4\pi}} \widehat{\frac{1}{2}} \widehat{S} \widehat{j_1} \widehat{j_2} \widehat{L} \widehat{J} \widehat{l_1} \\ (l_1 0 L 0 | l_2 0) \begin{Bmatrix} l_2 & \frac{1}{2} & j_2 \\ l_1 & \frac{1}{2} & j_1 \\ L & S & J \end{Bmatrix} R_{n_1 l_1 j_1}(r) R_{n_2 l_2 j_2}(r) \ . \quad (4.1)$$

**Initialization**

The module requires that the RPA amplitudes from the module `rpaAmps.f95` are read before the first call of `calcRho(L,S,J,N)` which calculates the density function for the quantum numbers $N$, $J$, $L$ and $S$. The density function values are stored in an internal data structure and can be received through consecutive calls to the function `getRho(r)` which returns the density function for the quantum numbers given in the last call of `calcRho(L,S,J,N)`

### Parameter

The header of the module defines the parameters for the step size and the radial range of the internal data structure.

```
RHO_R_STEP_SIZE  = 0.05_dp    ! fm
RHO_R_ARRAY_SIZE = 200        ! Samplepoints
```

### Testing

With the configuration option `TEST_DENSITY = 1` the density function of all RPA states will be written to the files `deb_rhoTest_NNN_J.txt` where `NNN` indicates the index of the state in the RPA file and `J` is the total angular momentum of the state. The files contain the density function and the radial integral of the density function

$$\int_0^r \mathrm{d}r' r'^2 \rho_{LSJ}^{J_N}(r')$$

## 4.5 alnucpot.f95

The module `alnucpot.f95` calculates the $\alpha$-nucleon potential in the multipole expansion given by

$$v_L(r_1, r_2) = 2\pi \int_{-1}^{1} \mathrm{d}(\cos\theta) P_L(\cos\theta) V(\sqrt{r_1^2 + r_2^2 - 2r_1 r_2 \cos\theta}) \tag{4.2}$$

$$V(r) = V_1 e^{-a_1 r^2} + V_2 e^{-a_2 r^2} \tag{4.3}$$

### Initialization

To calculate the $\alpha$-nucleon interaction the function `calcPotential()` has to be called. The interaction values are stored in an internal data structure and can be received through consecutive calls to the function `getPotential(l,r1,r2)` where `l` is the angular momentum.

### Parameter

The header of the module defines the parameters for the step size, the radial extent, the maximum angular momentum and the $\alpha$-nucleon potential parameters of Eq. (4.3)

```
ANPOT_R_STEP_SIZE  = 0.05_dp    ! fm
ANPOT_R_ARRAY_SIZE = 200        ! Samplepoints
ANPOT_MAX_L = 10                !
```

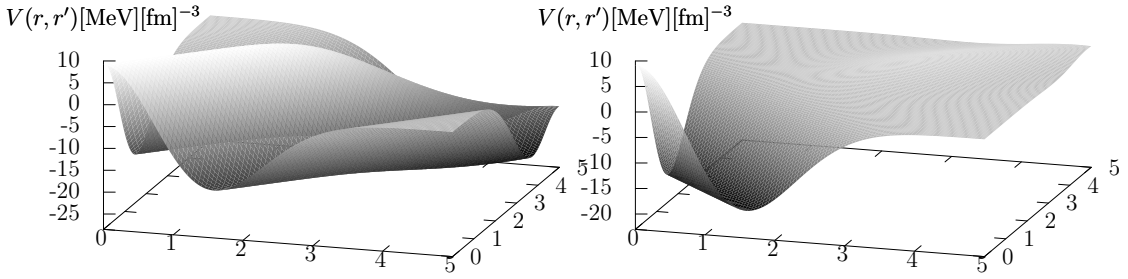


Figure 4.2: Sum of the radial $\alpha$-nucleon interaction for $\cos\theta = 1$ (left) and $\cos\theta = -1$ right

```
! Potential Parameter
V01    = -310.1_DP              ! MeV
V02    = 319.2_DP               ! MeV
alpha1 = 0.422_DP               ! 1/fm2
alpha2 = 0.505_DP               ! 1/fm2
```

**Testing**

With the configuration option `TEST_ALNUC_POTENTIAL = 1` the $\alpha$-nucleon potential for the direction $\cos\theta = 1$ and $\cos\theta = -1$ will be written to the file `deb_an_potential_sum.txt`. The file contains the sum of the multipole contribution up to $l =$ `ANPOT_MAX_L`.

$$V(r_1, r_2) = \sum_{l=0}^{\texttt{ANPOT\_MAX\_L}} \frac{(2l+1)}{4\pi}\, v_l(r_1, r_2) P_l(\cos\theta) \tag{4.4}$$

Fig.(4.2) shows that the sum reveals the original $\alpha$-nucleon potential of Eq. (4.3) along the diagonal $r_1 = r_2$ for $\cos\theta = 1$ and in perpendicular direction for $\cos\theta = -1$. Further, the test writes the first 4 multiple contributions for $\cos\theta = 1$ to `deb_an_potential_0-3.txt` as shown in Fig. 3.6.

## 4.6 `formfact.f95`

The module `formfact.f95` calculates from the nuclear density and the $\alpha$-nucleon interaction the transition form factor given by

$$F^D_{J_N,L0L}(r) = \int dr_1 r_1^2 \rho^{J_N}_{L0L}(r_1) v_L(r, r_1) \tag{4.5}$$

**Initialization**

To calculate the transition form factor the function `calcFormfact(N,L)` has to be called. The function calculates the form factor for the given index `N` of the RPA states and the angular momentum `L`. The results are stored in an internal data structure and can be received through consecutive calls to the function `getFormfact(r)`. Before the module can be used the RPA-amplitudes and the $\alpha$-nucleon interaction have to be initialized.

**Parameter**

The header of the module defines the parameters for the step size and the radial extent of the internal data structure.

```
FORM_R_STEP_SIZE   = 0.05_dp    ! fm
FORM_R_ARRAY_SIZE  = 200        ! Samplepoints
```

**Testing**

With the configuration option `WRITE_FORMFACTOR = 1` the transition form factors will be written to the files `deb_formfact_NNN_J.txt` where `NNN` indicates the index of the state in the RPA configuration file and `J` is the total angular momentum of the state.

## 4.7 intermedPot.f95

The module `intermdePot.f95` calculates the potential for the propagation in the intermediate states given as the double folding integral of the $\alpha$ and the $^{16}$O nucleon density distributions Eq. (3.12).

**Initialization**

To calculate the potential for the propagation in the intermediate state the function `initImPot()` has to be called. The results are stored in an internal data structure and can be received through consecutive calls to the function `getImPotR(e,r)`. The potential is internally calculated in steps of 10MeV up to 40MeV. The intermediate values are linearly interpolated.

**Parameter**

The header of the module defines the parameters for the step size and the radial extent of the internal data structure. The K-space parameters are for the internal array that holds the Fourier transformed functions before they are transformed back to the R-space.

```
IMPOT_R_STEP_SIZE  = 0.1        ! fm
IMPOT_R_ARRAY_SIZE = 100        ! SamplePoints
IMPOT_E_STEP_SIZE  = 10.0       ! MeV
IMPOT_E_ARRAY_SIZE = 4          ! Samplepoints

! K-Space Parameter
IMPOT_K_STEP_SIZE = 0.005_dp    ! 1/fm
IMPOT_K_ARRAY_SIZE = 400        ! Samplepoints
```

**Testing**

With the configuration option `TEST_INTERMEDPOT = 1` the potential will be written to the file `deb_intermedpot.txt`.

## 4.8 green.f95

The module `green.f95` calculates the radial Green function for the potential as described in Sec. 3.2.

**Initialization**

Prior the first usage of the module the function `initGreen()` has to be executed. This function will initialize the intermediate potential used for the Green function. To calculate the radial Green function for the angular momentum $l$ the function `calcGreen(energy, l)` has to be called. The results are then stored in an internal data structure and can be received through consecutive calls to the function `getGreen(r1,r2)`.

**Parameter**

The header of the module defines the parameter for the step size and the radial extend of the internal data structure.

```
GREEN_R_STEP_SIZE = 0.05_dp     ! fm
GREEN_R_ARRAY_SIZE = 200        ! Samplepoints
```

**Testing**

With the configuration option `TEST_GREEN = 1` the partial green function up to `MAX_L` will be written to the files `deb_green_EE_LL.txt` where `EE` will be replaced by the energy in the intermediate channel and `LL` will be the angular momentum. Further the sum of the partial Green function

$$\frac{\hbar^2}{2mk} \sum_{l=0}^{\infty} (2l+1)\ G_l(r,r')\ P_l(\cos\gamma) \tag{4.6}$$

is written to the file `deb_green_test.txt`. For the free particle option `GREEN_POT = 0` the sum has to reveal the form $\sin(ks)/ks$ and is shown in Fig. 4.3.

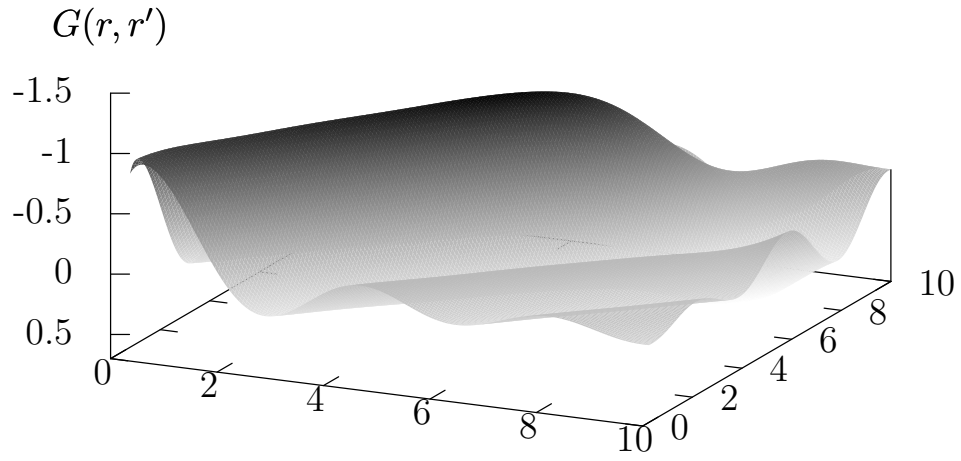


Figure 4.3: Sum of the radial Green function $G_l(r,r')$ up to l=10 normalized with the factor $2mk/\hbar^2$

## 4.9 optPot.f95

The module `optPot.f95` calculates the imaginary part of the optical potential by summing up the contributions from all open channels of

$$W(\vec{r},\vec{r}') = \mathrm{Im}\left[\frac{1}{16\pi^2}\sum_{\substack{l,l_c,L\\J_N}} \delta_{L,J_N}\frac{\widehat{l^2}\widehat{l_c^2}}{\widehat{L^2}}\,(l0l_c0|L0)\;\;,F^D_{J_N,L0L}(r)g_{l_c}(r,r')F^D_{J_N,L0L}(r')P_l(\cos\theta)\right], \tag{4.7}$$

### Initialization

Prior the first usage of the module the RPA amplitudes and the $\alpha$-$^{16}$O potential have to be initialized. The optical potential is calculated with a call to the function `calcOptPot(energy,cosTheta)` where `energy` is the $\alpha$ incident energy in the center of mass system and `cosTheta` is the $\cos\theta$ as used in Eq. (2.67). The potential is stored in the internal data structure and can be received by consecutive calls to `getOptPot(r1, r2)` which returns the real and the imaginary part of the calculation where only the imaginary part can be used for the optical potential.

### Parameter

The header of the module defines the parameter for the step size and the radial extend of the internal data structure.

```
OPTP_R_STEP_SIZE = 0.05_dp      ! fm
OPTP_R_ARRAY_SIZE = 200         ! Samplepoints
```

### Testing

The results from the calculation where used for nuclear cross section calculations and are discussed in Sec. 3.4.

# Part IV

# Appendix

# Appendix A

# Derivations

## A.1 Folding Potential

To calculate the double folding potential we insert Eq. (3.2) and Eq. (3.5) into Eq. (3.1) and get two double folding integrals

$$\begin{aligned} U(\vec{r}) &= \lambda\, C \left[ \int \mathrm{d}^3\vec{r}_1 \int \mathrm{d}^3\vec{r}_2 \; \rho_T(\vec{r}_1)\; \rho_\alpha(\vec{r}_2)\; g(\vec{r}+\vec{r}_1-\vec{r}_2) \right. \\ &+ \left. \alpha \int \mathrm{d}^3\vec{r}_1 \int \mathrm{d}^3\vec{r}_2 \; \rho_T(\vec{r}_1) e^{-\beta\rho_T(\vec{r}_2)}\; \rho_\alpha(\vec{r}_2) e^{-\beta\rho_\alpha(\vec{r}_2)}\; g(\vec{r}+\vec{r}_1-\vec{r}_2) \right] \end{aligned} \tag{A.1}$$

The calculation of the double folding integral is very time consuming thus we seek for a simpler way to calculate the integral for $U(\vec{r})$. From Eq. (A.1) we see that both integrals have the form

$$F(\vec{r}) = \int \mathrm{d}^3\vec{r}_1 \int \mathrm{d}^3\vec{r}_2 \; f_1(\vec{r}_1)\; f_2(\vec{r}_2)\; f_3(\vec{r}+\vec{r}_1-\vec{r}_2)\;. \tag{A.2}$$

To simplify Eq. (A.2) we perform a Fourier transformation. We keep the following derivation general in order not to imply restrictions on the functions $f_1$, $f_2$ and $f_3$ except that their Fourier transform must exist. Finally we restrict the functions to spherical symmetric ones so that we get the results for our purposes.

We rewrite Eq. (A.2) using Fourier transformed functions

$$\begin{aligned}
F(\vec{r}) &= \frac{1}{(2\pi)^{\frac{9}{2}}}\int \mathrm{d}^3\vec{r}_1 \int \mathrm{d}^3\vec{r}_2 \int \mathrm{d}^3\vec{k}_1 \int \mathrm{d}^3\vec{k}_2 \int \mathrm{d}^3\vec{k}_3 \\
&\quad \times \quad \tilde{f}_1(\vec{k}_1)\; e^{i\vec{k}_1\vec{r}_1}\tilde{f}_2(\vec{k}_2)\; e^{i\vec{k}_2\vec{r}_2}\tilde{f}_3(\vec{k}_3)e^{i\vec{k}_3(\vec{r}+\vec{r}_1-\vec{r}_2)} \\
&= (2\pi)^{\frac{3}{2}}\int \mathrm{d}^3\vec{k}_1 \int \mathrm{d}^3\vec{k}_2 \int \mathrm{d}^3\vec{k}_3 \\
&\quad \times \quad \tilde{f}_1(\vec{k}_1)\; \tilde{f}_2(\vec{k}_2)\; \tilde{f}_3(\vec{k}_3)e^{i\vec{k}_3\vec{r}}\delta^3(\vec{k}_1+\vec{k}_3)\delta^3(\vec{k}_2-\vec{k}_3) \\
&= (2\pi)^{\frac{3}{2}}\int \mathrm{d}^3\vec{k}\; \tilde{f}_1(-\vec{k})\; \tilde{f}_2(\vec{k})\; \tilde{f}_3(\vec{k})e^{i\vec{k}\vec{r}} \\
&= (2\pi)^3\frac{1}{(2\pi)^{\frac{3}{2}}}\int \mathrm{d}^3\vec{k}\widetilde{F}(k)e^{i\vec{k}\vec{r}} \qquad \text{(A.3)} \\
\widetilde{F}(\vec{k}) &= \tilde{f}_1(-\vec{k})\; \tilde{f}_2(\vec{k})\; \tilde{f}_3(\vec{k}) \qquad \text{(A.4)} \\
\tilde{f}(\vec{k}) &= \frac{1}{(2\pi)^{\frac{3}{2}}}\int \mathrm{d}^3\vec{r}\; f(\vec{r})\; e^{-i\vec{k}\vec{r}}\;. \qquad \text{(A.5)}
\end{aligned}$$

The functions $f_1$, $f_2$ and $f_3$ are spherical symmetric and therefore we can drop the angular dependence from Eq. (A.4) and simplify Eq. (A.5) to

$$\begin{aligned}
\widetilde{F}(k) &= \tilde{f}_1(k)\; \tilde{f}_2(k)\; \tilde{f}_3(k) \qquad \text{(A.6)} \\
\tilde{f}(k) &= \frac{1}{(2\pi)^{\frac{3}{2}}}\int \mathrm{d}^3\vec{r}\; f(r)\; e^{-i\vec{k}\vec{r}} \\
&= \frac{1}{(2\pi)^{\frac{1}{2}}}\int_0^\infty \mathrm{d}r\; r^2 f(r)\int_{-1}^1 \mathrm{d}(\cos\theta)e^{-ikr\cos\theta} \\
&= \frac{2}{(2\pi)^{\frac{1}{2}}}\int_0^\infty \mathrm{d}r\; r^2 f(r)\frac{\sin(kr)}{kr} \qquad \text{(A.7)} \\
F(r) &= (2\pi)^3\frac{2}{(2\pi)^{\frac{1}{2}}}\int_0^\infty \mathrm{d}k\; k^2\widetilde{F}(k)\frac{\sin(kr)}{kr}\;. \qquad \text{(A.8)}
\end{aligned}$$

With Eq. (A.6)-(A.8) we can rewrite Eq. (A.1) so we finally get the equation for the double folding integral

$$U(r) = \lambda C(2\pi)^3\mathrm{Ft}\Big[\mathrm{Ft}[g]\left(\mathrm{Ft}[\rho_T]\mathrm{Ft}[\rho_\alpha] + \alpha\mathrm{Ft}[\rho_T e^{-\beta\rho_T}]\mathrm{Ft}[\rho_\alpha e^{-\beta\rho_\alpha}]\right)\Big] \qquad \text{(A.9)}$$

$$\mathrm{Ft}[f] = \frac{2}{(2\pi)^{\frac{1}{2}}}\int_0^\infty \mathrm{d}r\; r^2 f(r)\frac{\sin(kr)}{kr} \qquad \text{(A.10)}$$

where $\mathrm{Ft}[f]$ is the 3 dimensional Fourier transform of the function $f$ given by Eq. (A.10). This expression is not a double folding integral but the Fourier transform of the product of 3 functions which themselves are Fourier transformed functions. For a function that is evaluated on a grid with $N$ sampling points the calculation effort reduces from $N^3$ to $4N^2$.

## A.2 The Green Function

Before we start with the discussion of the Green function let us recall briefly how the Green function was constructed,

$$G(\vec{r},\vec{r}') = \sum_{l=0}^{\infty} G_l(r,r')\frac{2l+1}{4\pi}P_l(\cos\gamma) \tag{A.11}$$

$$G_l(r,r') = N_l g_l(r,r') \tag{A.12}$$

$$g_l(r,r') = -\frac{1}{k}\phi_l(r_<)\psi_l(r_>)\ . \tag{A.13}$$

Here $G_l(r,r')$ is the radial Green function for the partial wave $l$ and $r_<$ and $r_>$ are the bigger and the smaller of the two radii $r$ and $r'$. $N_l$ is a complex scaling factor and $k = \sqrt{2\mu E_{\rm int}/\hbar^2}$ is the wave vector for the energy $E_{\rm int}$ in the intermediate channel. $\psi_l$ and $\phi_l$ are two independent solutions of the homogeneous Schrödinger equation

$$\begin{aligned}\widehat{H}\phi_l(r) &= 0\ ,\\ \widehat{H}\psi_l(r) &= 0\ ,\end{aligned} \tag{A.14}$$

with the Hamiltonian

$$\widehat{H} = -\frac{\hbar^2}{2\mu}\left[\frac{1}{r}\frac{\mathrm{d}^2}{\mathrm{d}r^2}r - \frac{l(l+1)}{r^2}\right] + V(r) - E_{\rm int}\ . \tag{A.15}$$

From the construction of the Green function it is clear that the application of the Hamilton operator to the Green function yields 0 except for $r = r'$

$$0 = \widehat{H}_l(r)\ G_l(r,r') \qquad \text{for} \quad r \neq r' \tag{A.16}$$

$$0 \neq \widehat{H}_l(r)\ G_l(r,r') \qquad \text{for} \quad r = r' \tag{A.17}$$

$$\tag{A.18}$$

The two functions $\phi(r)$ and $\psi(r)$ are independent continuous functions of $r$, thus $G_l(r,r')$ as well is a continuous function of $r$ and $r'$. From Eq. (A.11 - A.13) it is obvious that $G_l(r,r')$ is symmetric with respect to the exchange of its arguments $G_l(r,r') = G_l(r',r)$. As $\phi_l(r)$ and $\psi_l(r)$ are linearly independent the first derivative of $G_l(r,r')$ has a finite jump at $r = r'$ and the second derivative goes to infinity.

The boundary conditions

$$r\ G_l(r,r') \xrightarrow{r\to\infty} 0\ , \tag{A.19}$$

$$r\ G_l(r,r') \xrightarrow{r\to\infty} e^{ikr}\ , \tag{A.20}$$

imply that $\phi_l(r)$ and $\psi_l(r)$ fulfill the same boundary conditions

$$r\ \phi_l(r) \xrightarrow{r\to\infty} 0 \tag{A.21}$$

$$r\ \psi_l(r) \xrightarrow{r\to\infty} e^{ikr} \tag{A.22}$$

We choose the regular solution for $\phi_l(r)$ and the irregular solutions for $\psi_l(r)$. To fix the scaling factor $N_l$ we calculate the integral of Eq. (3.20).

$$\begin{aligned}
\frac{1}{r'^2} &= \int_0^\infty \mathrm{d}r \frac{1}{rr'}\delta(r-r') \\
&= N_l \int_0^\infty \mathrm{d}r \left(\widehat{H}_l(r) - E_{\mathrm{int}}\right) g(r,r') \\
&= N_l \lim_{\xi\to 0} \int_{r'-\xi}^{r'+\xi} \mathrm{d}r \left(\frac{\hbar^2}{2\mu}\left[\frac{1}{r}\frac{\mathrm{d}^2}{\mathrm{d}r^2}r - \frac{l(l+1)}{r^2}\right] + V(r) - E_{\mathrm{int}}\right) g(r,r') \\
&= N_l \frac{\hbar^2}{2\mu} \lim_{\xi\to 0} \int_{r'-\xi}^{r'+\xi} \mathrm{d}r \frac{1}{r}\frac{\mathrm{d}^2}{\mathrm{d}r^2} r g(r,r') \\
&= N_l \frac{\hbar^2}{2\mu} \lim_{\xi\to 0} \int_{r'-\xi}^{r'+\xi} \mathrm{d}r \frac{\mathrm{d}^2}{\mathrm{d}r^2} g(r,r') + \frac{2}{r}\frac{\mathrm{d}}{\mathrm{d}r} g(r,r') \\
&= N_l \frac{\hbar^2}{2\mu} \lim_{\xi\to 0} \int_{r'-\xi}^{r'+\xi} \mathrm{d}r \frac{\mathrm{d}^2}{\mathrm{d}r^2} g(r,r') \\
&= N_l \frac{\hbar^2}{2\mu} \lim_{\xi\to 0} \left(\frac{\mathrm{d}}{\mathrm{d}r} g(r,r')\bigg|_{r'+\xi} - \frac{\mathrm{d}}{\mathrm{d}r} g(r,r')\bigg|_{r'-\xi}\right) \\
&= -N_l \frac{\hbar^2}{2\mu}\frac{1}{k} \left(\phi_l(r') \frac{\mathrm{d}}{\mathrm{d}r}\psi_l(r)\bigg|_{r'} - \psi_l(r') \frac{\mathrm{d}}{\mathrm{d}r}\phi_l(r)\bigg|_{r'}\right) \qquad \text{(A.23)}
\end{aligned}$$

From Eq. (A.23) it seams that $N_l$ is not a constant but a function of $r'$ which is not the case. To show this we substitute $r\phi_l(r) = u_l(r)$ in Eq. (A.14) so that we get a new Schrödinger equation for $u_l(r)$.

$$\left[\frac{\mathrm{d}^2}{\mathrm{d}r^2} - \frac{l(l+1)}{r^2} + \frac{2\mu}{\hbar^2}\left(E_{\mathrm{int}} - U(r)\right)\right] u_l(r) = 0 \ . \qquad \text{(A.24)}$$

We do the same for $r\psi_l(r) = v_l(r)$ and inset the result into Eq. (A.23)

$$\begin{aligned}
\frac{2\mu}{\hbar^2}\frac{1}{N_l} &= \left(u_l(r)\frac{rv_l'(r) + v_l(r)}{r} - v_l(r)\frac{ru_l'(r) + u_l(r)}{r}\right) \\
&= u_l(r)v_l'(r) - u_l'(r)v_l(r) \ . \qquad \text{(A.25)}
\end{aligned}$$

We have introduced the notation $u_l'(r) = \frac{\mathrm{d}}{\mathrm{d}r}u_l(r)$ and replaced $r'$ by $r$. To demonstrate that $N_l$ is independent from $r$ we show that the derivative of the right hand side of Eq. (A.25) vanishes for all $r$. Using Eq. (A.24) we can replace the second derivatives $u_l''(r)$ and $v_l''(r)$ to get the desired result.

$$\begin{aligned}
-\frac{2\mu}{\hbar^2}\frac{\mathrm{d}}{\mathrm{d}r}\frac{k}{N_l} &= \left(u_l(r)v_l'(r) - u_l'(r)v_l(r)\right)' \\
&= u_l(r)v_l''(r) - u_l''(r)v_l(r) \\
&= \left[\frac{l(l+1)}{r^2} - \frac{2\mu}{\hbar^2}\left(E_{\mathrm{int}} - U(r)\right)\right]\left(u_l(r)v_l(r) - u_l(r)v_l(r)\right) \\
&= 0 \qquad \text{(A.26)}
\end{aligned}$$

We see from Eq. (A.26) that the scaling factor $N_l$ is independent from the radius $r$ and can be evaluated at any distance via

$$N_l = \frac{2\mu}{\hbar^2}\frac{k}{r'^2}\left(\phi_l(r')\left.\frac{\mathrm{d}}{\mathrm{d}r}\psi_l(r)\right|_{r'} - \psi_l(r')\left.\frac{\mathrm{d}}{\mathrm{d}r}\phi_l(r)\right|_{r'}\right)^{-1} . \tag{A.27}$$

## A.3 Spherical Multipole Expansion of the Nuclear Interaction

The central $\alpha$-target interaction $v_L(r_1, r_2)$ in Eq. (2.68) arises from the multipole expansion

$$V(\vec{r}) = \sum_{l=0}^{\infty}\frac{(2l+1)}{4\pi}v_l(r_1, r_2)P_l(\cos\theta) , \tag{A.28}$$

where $P_l(\cos\theta)$ are the Legendre polynomials and $\theta$ is the angle between $\vec{r}_1$ and $\vec{r}_2$ and $\vec{r} = \vec{r}_2 - \vec{r}_1$. We search for an expression for $v_l(r_1, r_2)$ as a function of $V(r)$ and start by expressing $V(\vec{r})$ by it's spherical Fourier transform

$$\widetilde{V}(\vec{k}) = \frac{1}{(2\pi)^3}\int \mathrm{d}^3\vec{r}\; V(r)e^{i\vec{k}\vec{r}} . \tag{A.29}$$

With the help of

$$e^{i\vec{k}\vec{r}} = 4\pi\sum_{l=0}^{\infty} i^l j_l(kr)\sum_{m=-l}^{l} Y_{lm}(\hat{r})Y_{lm}(\hat{k}) , \tag{A.30}$$

where $j_l(kr)$ are the spherical Bessel functions, we get

$$\widetilde{V}(k) = \frac{1}{2\pi^2}\int_0^{\infty}\mathrm{d}r\; r^2V(r)j_0(kr) . \tag{A.31}$$

The angular integral over the $Y_{lm}$ cancels all contributions from $l \neq 0$ and the interaction in the $k$ space is also spherical symmetric thus we drop the vector sign from $k$. Performing the inverse Fourier transform on Eq. (A.31) yields

$$\begin{aligned} V(r) &= \int \mathrm{d}^3\vec{k}\; \widetilde{V}(k)e^{-i\vec{k}\vec{r}_2}e^{i\vec{k}\vec{r}_1} \\ &= (4\pi)^2\int \mathrm{d}^3\vec{k}\; \widetilde{V}(k)\sum_{l_1m_1}\sum_{l_2m_2} i^{l_1+l_2}\; j_{l_1}(-kr_2)\; j_{l_2}(kr_1) \\ &\qquad \times\quad Y_{l_1m_1}(\hat{r}_2)\; Y_{l_1m_1}(\hat{k})\; Y_{l_2m_2}(\hat{r}_1)\; Y_{l_2m_2}(\hat{k}) \\ &= (4\pi)^2\int_0^{\infty}\mathrm{d}k\; k^2\widetilde{V}(k)\sum_{lm}(-1)^l j_l(-kr_2)\; j_l(kr_1)\; Y_{lm}(\hat{r}_2)\; Y_{lm}(\hat{r}_1) , \end{aligned} \tag{A.32}$$

where we replaced $\vec{r} = \vec{r}_2 - \vec{r}_1$ and use the spherical wave expansion from Eq. (A.30). With the addition theorem of the spherical harmonics

$$\sum_{m=-l}^{l} Y_{lm}(r_1)\ Y_{lm}(r_2) = \frac{2l+1}{4\pi} P_l(\cos\theta)\ , \tag{A.33}$$

we get the expression

$$V(r) = \sum_{l} \frac{(2l+1)}{4\pi} v_l(r_1, r_2) P_l(\cos\theta)\ , \tag{A.34}$$

with

$$v_l(r_1, r_2) = (4\pi)^2(-1)^l \int_0^\infty \mathrm{d}k\ k^2 \widetilde{V}(k) j_l(-kr_2)\ j_l(kr_1)\ . \tag{A.35}$$

We replace in Eq. (A.35) the $k$-space potential by its Fourier transformation Eq. (A.31) and obtain

$$v_l(r_1, r_2) = 8(-1)^l \int_0^\infty \mathrm{d}r\ r^2 V(r) \int_0^\infty \mathrm{d}k\ k^2 j_0(kr)\ j_l(kr_1)\ j_l(-kr_2)\ . \tag{A.36}$$

The integral of 3 spherical Bessel function has the analytic solution[27]

$$\int_0^\infty \mathrm{d}k\ k^2 j_0(kr)\ j_l(kr_1)\ j_l(kr_2) = (-1)^l \frac{\pi}{4r\ r_1 r_2} P_l(\cos\theta) \tag{A.37}$$

where $\theta$ is the angle between $\vec{r}_1$ and $\vec{r}_2$. Substitution of Eq. (A.37) in Eq. (A.36) yields

$$v_l(r_1, r_2) = 2\pi \int_0^\infty \mathrm{d}r\ r^2 V(r) \frac{1}{r\ r_1 r_2} P_l(\cos\theta) \tag{A.38}$$

The integral over the whole range of $r$ can be evaluated when we take into account that due to $\vec{r} = \vec{r}_2 - \vec{r}_1$ the triangular relation $|r_1 - r_2| \leq r \leq |r_1 + r_2|$ has to be satisfied. Thus we substitute

$$r = \sqrt{r_1^2 + r_2^2 - 2r_1 r_2 \cos\theta} \tag{A.39}$$

with

$$\cos\theta = \frac{r_1^2 + r_2^2 - r^2}{2r_1 r_2}\ . \tag{A.40}$$

Finally we get for the spherical multipole expansion of the nuclear interaction

$$v_l(r_1, r_2) = 2\pi \int_{-1}^{1} \mathrm{d}(\cos\theta)\ V(r) P_l(\cos\theta)\ . \tag{A.41}$$

# Appendix B

# Tables

## B.1 $^{16}$0 RPA Amplitudes

| | | E= | 6.52 MeV | | 18.91 MeV | | 46.99 MeV | | 54.65 MeV | |
|---|---|---|---|---|---|---|---|---|---|---|
| T | h | p | X | Y | X | Y | X | Y | X | Y |
| 0 | $1s_{\frac{1}{2}}$ | $1f_{\frac{7}{2}}$ | -0.062 | -0.059 | 0.030 | 0.002 | 0.065 | 0.022 | 0.393 | -0.001 |
| | | $1f_{\frac{5}{2}}$ | 0.053 | 0.032 | -0.001 | -0.011 | -0.145 | -0.000 | -0.037 | 0.015 |
| | $1p_{\frac{3}{2}}$ | $1d_{\frac{5}{2}}$ | -0.293 | -0.146 | -0.723 | 0.013 | -0.036 | 0.027 | 0.038 | -0.010 |
| | | $1d_{\frac{3}{2}}$ | 0.281 | 0.118 | -0.008 | -0.035 | 0.143 | 0.001 | 0.011 | 0.036 |
| | | $1g_{\frac{9}{2}}$ | 0.123 | 0.111 | -0.050 | -0.004 | -0.847 | -0.042 | -0.371 | 0.001 |
| | $1p_{\frac{1}{2}}$ | $1d_{\frac{5}{2}}$ | 0.653 | 0.240 | 0.184 | -0.001 | -0.002 | -0.054 | -0.061 | -0.005 |
| 1 | $1s_{\frac{1}{2}}$ | $1f_{\frac{7}{2}}$ | -0.062 | -0.062 | -0.030 | -0.002 | 0.224 | 0.020 | -0.708 | -0.004 |
| | | $1f_{\frac{5}{2}}$ | 0.057 | 0.033 | -0.001 | 0.012 | -0.107 | -0.010 | 0.090 | -0.015 |
| | $1p_{\frac{3}{2}}$ | $1d_{\frac{5}{2}}$ | -0.311 | -0.156 | 0.635 | -0.013 | 0.063 | 0.032 | -0.029 | 0.004 |
| | | $1d_{\frac{3}{2}}$ | 0.246 | 0.101 | -0.004 | 0.029 | 0.102 | -0.021 | -0.029 | -0.028 |
| | | $1g_{\frac{9}{2}}$ | 0.085 | 0.079 | 0.030 | 0.002 | -0.410 | 0.027 | 0.436 | 0.005 |
| | $1p_{\frac{1}{2}}$ | $1d_{\frac{5}{2}}$ | 0.661 | 0.258 | -0.195 | -0.001 | 0.047 | -0.045 | 0.058 | 0.015 |

Table B.1: $^{16}$O RPA amplitudes $3^-$ states from S. Krewald and J. Speth[20]

| | | E= | 14.1 MeV | | 18.33 MeV | | 19.97 MeV | | 22.22 MeV | |
|---|---|---|---|---|---|---|---|---|---|---|
| T | h | p | X | Y | X | Y | X | Y | X | Y |
| 0 | $1s_{\frac{1}{2}}$ | $2p_{\frac{3}{2}}$ | -0.030 | -0.001 | -0.016 | -0.002 | 0.045 | 0.016 | -0.026 | -0.005 |
| | | $2p_{\frac{1}{2}}$ | -0.008 | 0.017 | -0.000 | 0.001 | -0.032 | 0.003 | 0.004 | 0.010 |
| | $1p_{\frac{3}{2}}$ | $1d_{\frac{5}{2}}$ | 0.030 | 0.008 | -0.028 | 0.010 | 0.022 | 0.006 | -0.647 | 0.039 |
| | | $2s_{\frac{1}{2}}$ | 0.008 | -0.025 | -0.266 | -0.011 | -0.568 | 0.003 | 0.076 | 0.012 |
| | | $1d_{\frac{3}{2}}$ | -0.015 | -0.000 | -0.059 | 0.004 | -0.058 | 0.003 | 0.164 | -0.034 |
| | $1p_{\frac{1}{2}}$ | $2s_{\frac{1}{2}}$ | -0.420 | -0.012 | -0.068 | -0.005 | -0.029 | -0.030 | 0.037 | -0.004 |
| | | $1d_{\frac{3}{2}}$ | -0.074 | -0.004 | 0.152 | -0.001 | 0.035 | 0.001 | 0.200 | -0.053 |
| 1 | $1s_{\frac{1}{2}}$ | $2p_{\frac{3}{2}}$ | 0.036 | -0.010 | -0.018 | 0.010 | 0.004 | -0.018 | 0.026 | 0.003 |
| | | $2p_{\frac{1}{2}}$ | 0.027 | -0.024 | -0.024 | 0.012 | 0.036 | -0.007 | 0.001 | -0.011 |
| | $1p_{\frac{3}{2}}$ | $1d_{\frac{5}{2}}$ | 0.136 | 0.009 | -0.174 | -0.042 | -0.131 | -0.013 | 0.655 | -0.035 |
| | | $2s_{\frac{1}{2}}$ | -0.088 | 0.038 | -0.374 | -0.012 | 0.786 | 0.006 | 0.098 | -0.013 |
| | | $1d_{\frac{3}{2}}$ | 0.004 | -0.007 | 0.202 | -0.016 | 0.138 | -0.010 | -0.223 | 0.031 |
| | $1p_{\frac{1}{2}}$ | $2s_{\frac{1}{2}}$ | 0.888 | 0.033 | -0.075 | -0.003 | 0.085 | 0.040 | -0.042 | 0.006 |
| | | $1d_{\frac{3}{2}}$ | -0.050 | -0.010 | -0.826 | -0.002 | -0.109 | -0.005 | -0.166 | 0.044 |

Table B.2: $^{16}$O RPA amplitudes $1^-$ states from S. Krewald and J. Speth[20]

| | | E= | 27.64 MeV | | 38.49 MeV | | 43.28 MeV | |
|---|---|---|---|---|---|---|---|---|
| T | h | p | X | Y | X | Y | X | Y |
| 0 | $1s_{\frac{1}{2}}$ | $2s_{\frac{1}{2}}$ | 0.126 | 0.020 | 0.012 | -0.000 | -0.510 | 0.034 |
| | $1p_{\frac{3}{2}}$ | $2p_{\frac{3}{2}}$ | -0.420 | -0.055 | 0.444 | -0.016 | 0.383 | -0.036 |
| | $1p_{\frac{1}{2}}$ | $2p_{\frac{1}{2}}$ | 0.558 | 0.040 | -0.123 | 0.012 | -0.174 | 0.026 |
| 1 | $1s_{\frac{1}{2}}$ | $2s_{\frac{1}{2}}$ | 0.104 | 0.018 | -0.673 | -0.004 | 0.628 | -0.033 |
| | $1p_{\frac{3}{2}}$ | $2p_{\frac{3}{2}}$ | -0.426 | -0.055 | -0.560 | 0.020 | -0.381 | 0.036 |
| | $1p_{\frac{1}{2}}$ | $2p_{\frac{1}{2}}$ | 0.561 | 0.039 | 0.152 | -0.014 | 0.169 | -0.026 |

Table B.3: $^{16}$O RPA amplitudes $0^+$ states from S. Krewald and J. Speth[20]

| | | E= | 23.04 MeV | | 29.94 MeV | | 41.14 MeV | |
|---|---|---|---|---|---|---|---|---|
| T | h | p | X | Y | X | Y | X | Y |
| 0 | $1s_{\frac{1}{2}}$ | $1g_{\frac{9}{2}}$ | 0.020 | 0.023 | 0.011 | 0.007 | -0.064 | 0.004 |
| | $1p_{\frac{3}{2}}$ | $1f_{\frac{7}{2}}$ | 0.136 | 0.033 | 0.790 | 0.010 | 0.104 | -0.002 |
| | | $1f_{\frac{5}{2}}$ | -0.164 | -0.016 | -0.084 | -0.007 | 0.879 | 0.029 |
| | $1p_{\frac{1}{2}}$ | $1f_{\frac{7}{2}}$ | -0.792 | -0.055 | 0.077 | -0.015 | -0.126 | -0.010 |
| 1 | $1s_{\frac{1}{2}}$ | $1g_{\frac{9}{2}}$ | 0.019 | 0.015 | 0.018 | 0.004 | -0.034 | -0.003 |
| | $1p_{\frac{3}{2}}$ | $1f_{\frac{7}{2}}$ | 0.171 | 0.034 | 0.501 | 0.012 | 0.134 | -0.010 |
| | | $1f_{\frac{5}{2}}$ | -0.149 | -0.025 | -0.060 | -0.022 | 0.405 | 0.026 |
| | $1p_{\frac{1}{2}}$ | $1f_{\frac{7}{2}}$ | -0.525 | -0.051 | 0.331 | -0.011 | -0.126 | 0.005 |

Table B.4: $^{16}$O RPA amplitudes $4^+$ states from S. Krewald and J. Speth[20]

| | | E= | 22.97 MeV | | 34.72 MeV | | 36.22 MeV | | 41.26 MeV | |
|---|---|---|---|---|---|---|---|---|---|---|
| T | h | p | X | Y | X | Y | X | Y | X | Y |
| 0 | $1s_{\frac{1}{2}}$ | $1d_{\frac{5}{2}}$ | -0.190 | -0.053 | 0.083 | -0.007 | 0.392 | 0.014 | 0.296 | -0.006 |
| | | $1d_{\frac{3}{2}}$ | 0.133 | 0.032 | 0.073 | -0.004 | -0.146 | -0.003 | 0.179 | 0.013 |
| | $1p_{\frac{3}{2}}$ | $1f_{\frac{7}{2}}$ | 0.606 | 0.098 | 0.079 | 0.001 | 0.128 | -0.021 | -0.078 | 0.017 |
| | | $1f_{\frac{5}{2}}$ | -0.129 | -0.025 | -0.111 | 0.006 | 0.182 | 0.001 | 0.636 | -0.002 |
| | | $2p_{\frac{3}{2}}$ | 0.051 | 0.011 | -0.013 | -0.000 | 0.061 | 0.003 | 0.038 | -0.003 |
| | | $2p_{\frac{1}{2}}$ | -0.038 | -0.010 | 0.008 | -0.000 | 0.071 | 0.001 | 0.288 | 0.016 |
| | $1p_{\frac{1}{2}}$ | $1f_{\frac{5}{2}}$ | -0.343 | -0.058 | 0.748 | 0.004 | -0.457 | 0.007 | 0.120 | -0.008 |
| | | $2p_{\frac{3}{2}}$ | -0.096 | -0.012 | -0.002 | 0.003 | -0.013 | -0.002 | -0.115 | -0.013 |
| 1 | $1s_{\frac{1}{2}}$ | $1d_{\frac{5}{2}}$ | -0.186 | -0.053 | 0.300 | 0.002 | 0.382 | -0.001 | -0.424 | -0.003 |
| | | $1d_{\frac{3}{2}}$ | 0.106 | 0.027 | 0.002 | -0.010 | 0.021 | -0.007 | 0.136 | -0.013 |
| | $1p_{\frac{3}{2}}$ | $1f_{\frac{7}{2}}$ | 0.539 | 0.010 | 0.545 | -0.004 | 0.230 | 0.002 | 0.134 | -0.005 |
| | | $1f_{\frac{5}{2}}$ | -0.126 | -0.027 | -0.040 | 0.013 | -0.071 | 0.009 | -0.165 | 0.009 |
| | | $2p_{\frac{3}{2}}$ | 0.061 | 0.013 | -0.031 | -0.001 | -0.188 | 0.001 | -0.012 | 0.001 |
| | | $2p_{\frac{1}{2}}$ | -0.044 | -0.011 | -0.011 | 0.001 | -0.060 | 0.009 | -0.319 | -0.015 |
| | $1p_{\frac{1}{2}}$ | $1f_{\frac{5}{2}}$ | -0.313 | -0.061 | 0.143 | 0.016 | 0.562 | 0.010 | -0.047 | 0.012 |
| | | $2p_{\frac{3}{2}}$ | -0.115 | -0.015 | -0.021 | -0.001 | 0.007 | -0.002 | 0.112 | 0.016 |

Table B.5: $^{16}$O RPA amplitudes $2^+$ states from S. Krewald and J. Speth[20]

| | | E= | 13.36 MeV | | 22.79 MeV | | 24.73 MeV | | 25.32 MeV | |
|---|---|---|---|---|---|---|---|---|---|---|
| T | h | p | X | Y | X | Y | X | Y | X | Y |
| 0 | $1s_{\frac{1}{2}}$ | $1f_{\frac{5}{2}}$ | 0.006 | 0.004 | -0.033 | -0.015 | 0.021 | 0.009 | -0.030 | -0.012 |
| | | $2p_{\frac{3}{2}}$ | -0.020 | -0.012 | -0.020 | -0.008 | -0.017 | -0.006 | 0.030 | 0.011 |
| | $1p_{\frac{3}{2}}$ | $1d_{\frac{5}{2}}$ | 0.289 | 0.041 | -0.532 | 0.045 | -0.121 | 0.020 | 0.244 | -0.042 |
| | | $2s_{\frac{1}{2}}$ | 0.036 | 0.006 | -0.173 | 0.019 | -0.038 | 0.006 | 0.083 | -0.013 |
| | | $1d_{\frac{3}{2}}$ | 0.084 | 0.022 | 0.177 | 0.001 | -0.573 | 0.021 | 0.724 | -0.035 |
| | $1p_{\frac{1}{2}}$ | $1d_{\frac{5}{2}}$ | -0.841 | 0.063 | -0.176 | 0.058 | -0.104 | 0.038 | 0.190 | -0.072 |
| | | $1d_{\frac{3}{2}}$ | -0.043 | -0.005 | -0.371 | 0.058 | 0.108 | -0.021 | -0.126 | 0.026 |
| 1 | $1s_{\frac{1}{2}}$ | $1f_{\frac{5}{2}}$ | 0.004 | 0.002 | 0.029 | 0.014 | 0.020 | 0.009 | 0.019 | 0.008 |
| | | $2p_{\frac{3}{2}}$ | -0.010 | -0.010 | 0.014 | 0.006 | -0.020 | -0.008 | -0.020 | -0.008 |
| | $1p_{\frac{3}{2}}$ | $1d_{\frac{5}{2}}$ | 0.146 | 0.020 | 0.517 | -0.066 | -0.210 | -0.035 | -0.213 | 0.038 |
| | | $2s_{\frac{1}{2}}$ | 0.017 | 0.003 | 0.226 | -0.023 | -0.087 | 0.012 | -0.090 | 0.014 |
| | | $1d_{\frac{3}{2}}$ | 0.034 | 0.009 | -0.246 | -0.003 | -0.747 | 0.021 | -0.536 | 0.022 |
| | $1p_{\frac{1}{2}}$ | $1d_{\frac{5}{2}}$ | -0.429 | 0.031 | 0.186 | -0.061 | -0.156 | 0.057 | -0.159 | 0.059 |
| | | $1d_{\frac{3}{2}}$ | -0.022 | -0.002 | 0.306 | -0.042 | 0.074 | -0.013 | 0.060 | -0.011 |

Table B.6: $^{16}$O RPA amplitudes $2^-$ states from S. Krewald and J. Speth[20]

# Bibliography


[1] N. R. C. Astronomy and A. in the New Millennium, *Commission on Physical Sciences, Mathematics, and Applications* (National Academy Press, Washington, D.C., 2001).

[2] F. Feshbach, Ann. Phys. (N.Y.) **5**, 357 (1958).

[3] F. Osterfeld, J.Wambach, and V. Madsen, Phys. Rev. C **23**, 179 (1981).

[4] I. Levine, *Quantum Chemistry* (Prentice Hall, Englewood Cliffs, New Jersey, 1991), pp. 455–544.

[5] C. Cramer, *Essentials of Computational Chemistry* (John Wiley & Sons, Ltd., Chichester, 2002), pp. 153–189.

[6] J. Slater, Phys. Rev. **34**, 1293 (1929).

[7] P. Dirac, *The Principles of Quantum Mechanics: 4TH EDITION* (University Press, Oxford, 1981).

[8] J. Bell, Nucl. Phys. **12**, 117 (1959).

[9] A.L.Fettter and J.D.Walecka, *Quantum Theory of Many-Particle Systems* (Dover Publications Ind., Mineola, New York, 2003).

[10] D. Bohm and D. Pines, Phys. Rev. **92**, 609 (1953).

[11] D. Pines, Phys. Rev. **92**, 626 (1953).

[12] R. Kogler, Master's thesis, Vienna University of Technology, 2006.

[13] P. Fröbrich and R. Lipperheide, *Theory of Nuclear Reactions* (Clarendon Press, Oxford, 1996).

[14] H. Hodgson, *The Nucleon Optical Model* (World Scientific Publishing, Singapore, 1994).

[15] C. Rao, M.Reeves, and G. Satchler, Nucl. Phys. **A207**, 182 (1973).

[16] F. Feshbach, Ann. Phys. (N.Y.) **19**, 257 (1962).

[17] H. Dermawan, F. Osterfeld, and V. Madsen, Phys. Rev. C **25**, 180 (1982).

[18] H. Leeb and F. Osterfeld, Phys. Rev. C **23**, 789 (1985).

[19] F. Villars, in *Fundamentals of Nuclear Theory*, edited by A. de Shalit and C. Villi (IAEA, Vienna, 1967).

[20] S. Krewald and J. Speth, Phys. Lett. B **52**, 295 (1974).

[21] G. Bertsch, J. Borysowicz, H. McManus, and W. Love, Nucl. Phys. **A284**, 399 (1977).

[22] A. M. Kobos *et al.*, Nucl. Phys. **A384**, 65 (1982).

[23] A. Kobos, B. Brown, R. Lindsay, and G. Satchler, Nucl. Phys. **A425**, 205 (1984).

[24] H. de Vries et al., Atomic Data and Nuclear Data Tables **36**, 496 (1987).

[25] V. Gillet and E. A. Sanderson, Nucl. Phys. **A91**, 292 (1967).

[26] J. C. Corelli, E. Bleuler, and D. J. Tendam, Phys. Rev. **116**, 1164 (1959).

[27] R. Mehrem, J. Londergan, and M. Macrarlane, J. Phys.A: Math. Gen. **24**, 1435 (1991).

[28] S. Woosley, A. Heger, T. Rauscher, and R. Hoffmann, Nucl. Phys. **A718**, 3c (2003).

[29] R. Woods and D. Saxon, Phys. Rev. **95**, 577 (1954).

[30] H. Feshbach, C. Porter, and V. Weisskopf, Phys. Rev. **96**, 448 (1954).

[31] C. Mahaux and H. Weidenmüller, *Shell model approach to nuclear reactions* (North-Holland, Amsterdam, 1969).

[32] H. Horie and K. Sasaki, Prog. of Th. Phys. **25**, 475 (1961).

[33] K. L. Heyde, *The nuclear Shell Model* (Springer Verlag, Berlin Heidelberg New York, 1994).

## Acknowledgment

This diploma thesis it the last step on my long journey towards my degree in physics. I never would have been able to achieve this goal without the help of my fellow friends and colleagues and I would like to thank all those who have accompanied me on this way.

Particularly I would like to express my gratitude towards Prof. Helmut Leeb for patiently answering my questions even during his busiest hours and for his incredible helpful support in the finalization of this work. I admire him for his profound knowledge and his excellent skills as a teacher.

I further would like to thank Hermann Bühler for the patience he had whenever I fell short of my duties due to excessive studies. Great thanks go also to his wife Eva Buchinger-Bühler for her countless reminders to pull myself together and bring my studies to an end.

Here I also would like to say thank you to all my friends and colleagues who have inspired and encouraged me through all the years.

And last but not least my special thanks go towards my parents. I am very glad to say that I am looking back to a really well protected lovely childhood which brought me to the place where I stand now. Definitely this will not be the end of my journey but just the beginning of a new phase of my life. I wish that some day I can pass on to my kids all the passion and affection you gave to me.

My sincere thanks go to all of you,

family, friends and colleagues!

Michel Feher